REPORT DOCUMENTATION PAGE			Form Approved OMB No. 0704-0188

Public reporting burden for this collection of information is estimated to average 1 hour per response, including the time for reviewing instructions, searching existing data sources, gathering and maintaining the data needed, and completing and reviewing the collection of information. Send comments regarding this burden estimate or any other aspect of this collection of information, including suggestions for reducing this burden, to Washington Headquarters Services, Directorate for Information Operations and Reports, 1215 Jefferson Davis Highway, Suite 1204, Arlington, VA 22202-4302, and to the Office of Management and Budget, Paperwork Reduction Project (0704-0188), Washington, DC 20503.

1. AGENCY USE ONLY *(Leave blank)*	2. REPORT DATE	3. REPORT TYPE AND DATES COVERED
	21.Jun.04	MAJOR REPORT

4. TITLE AND SUBTITLE
DIAGNOSIS OF MEDIUM-RANGE PREDICTABILITY ENHANCEMENT DURING ANOMALOUS WINTER ZONAL FLOWS OVER WESTERN NORTH AMERICA

5. FUNDING NUMBERS

6. AUTHOR(S)
MAJ BYERLE LEE A

7. PERFORMING ORGANIZATION NAME(S) AND ADDRESS(ES)
UNIVERSITY OF UTAH

8. PERFORMING ORGANIZATION REPORT NUMBER
CI04-385

9. SPONSORING/MONITORING AGENCY NAME(S) AND ADDRESS(ES)
THE DEPARTMENT OF THE AIR FORCE
AFIT/CIA, BLDG 125
2950 P STREET
WPAFB OH 45433

10. SPONSORING/MONITORING AGENCY REPORT NUMBER

11. SUPPLEMENTARY NOTES

12a. DISTRIBUTION AVAILABILITY STATEMENT
Unlimited distribution
In Accordance With AFI 35-205/AFIT Sup

DISTRIBUTION STATEMENT A
Approved for Public Release
Distribution Unlimited

12b. DISTRIBUTION CODE

13. ABSTRACT *(Maximum 200 words)*

20040709 072

BEST AVAILABLE COPY

14. SUBJECT TERMS			15. NUMBER OF PAGES 45
			16. PRICE CODE
17. SECURITY CLASSIFICATION OF REPORT	18. SECURITY CLASSIFICATION OF THIS PAGE	19. SECURITY CLASSIFICATION OF ABSTRACT	20. LIMITATION OF ABSTRACT

Diagnosis of medium-range predictability enhancement during anomalous winter zonal flows over western North America

Lee A. Byerle and Jan Paegle

Department of Meteorology
University of Utah
Salt Lake City, UT 84112

DISTRIBUTION STATEMENT A
Approved for Public Release
Distribution Unlimited

Abstract

This investigation analyzes medium range predictability enhancement during winter cases of anomalous, upper troposphere zonal flows over western North America. Time correlations based upon a 50 year record of reanalyses suggest that winters with anomalously strong zonal winds are wetter over the region, while years with anomalously weak zonal winds are relatively drier. Forecasts are selected based upon anomalously weak and strong zonal flows during January. Results from 15 day simulations using a variety of operational and research global model configurations are presented to diagnose the predictability of precipitation and large scale features. Model forecasts of precipitation accumulation delineate qualitatively between wet and dry events at both 5 and 10 days. Anomaly correlations of the geopotential height field reveal useful predictability for some ensembles extending to 9.5 days. Uniform resolution forecasts are compared with two model configurations which employ rotated variable resolution. Uniform and variable resolution forecasts maintain representative precipitation into the second week over the western U.S. The rotated variable resolution simulations provide more precipitation detail. Diagnostics and model simulations of a small number of extreme events suggest that flow modifications associated with ambient flows exist over the orography during the winter season, and that a predictable regional response may be present to about 10 days. The persistence of the anomalies may also contribute to the improved model performance in certain cases. Improved performance may be related to the large inertia of the flow in wet events, and to the persistence and increased predictability of initial, large scale anomalies in both wet and dry events. Present conclusions are limited by the small case sampling, which will be expanded in future investigations.

1. Introduction

Precipitation prediction has remained a difficult challenge on both climate and shorter scales (e.g., 12-36 hours). The status as of the late 1990s was given by the Prospectus Development team of the U.S. Weather Research Program [*Fritsch et al.*, 1998]. They discussed the "[very slow rate of improvement]" in quantitative precipitation forecasting (QPF) during the preceding decade. The complexity of orography, such as that over western North America, adds to the forecast challenge, and has been the subject of various field campaigns during recent winters. Orographic precipitation processes in Oregon's Cascade Mountains were a component of the Improvement of Microphysical Parametrization through Observational verification field experiment (IMPROVE) [*Stoelinga et al.*, 2003]. The Intermountain Precipitation Experiment (IPEX) focused on the Great Basin during February 2000 [*Schultz et al.*, 2002]. *Gartner et al.* [1996] partly motivated IPEX in documenting that Eta model QPF skill over the Intermountain West and eastern Rocky Mountains ranked the lowest in the U.S.

Smith et al. [1997] identified research needs and opportunities in mountain meteorology and summarized some of the difficulties in QPF and verification over complex terrain. They pointed out that while topography may locally enhance precipitation predictability by organizing precipitation, small shifts in ambient flows, which may be undetected in models, will cause a shift in which slopes favor heavy precipitation.

White et al. [1999] highlighted the difficulty of forecast verification over the western U.S., where raw observations themselves may often have gaps of many kilometers and subsequent gridded observations may contain lower resolution than forecast models. Medium-range precipitation prediction (order of 10 days) over western North America has not received as much

attention as prediction at shorter and longer (e.g., El Niño Southern Oscillation (ENSO)) time scales.

This investigation presents two-week forecasts in winter cases of chosen anomalous, upper troposphere zonal flows over western North America. Results using a variety of global model configurations are presented to diagnose model performance of precipitation and large scale features.

The importance of second week prediction of extreme events for both societal and economic benefit has been recognized by scientists involved in THORPEX, an international research program [*Shapiro et al.*, 2003 and references therein]. Goals of THORPEX include improving "high-impact" weather forecasts in the 1-14 day range. *Shapiro et al.* [2003] and others [e.g., *Simmons and Hollingsworth*, 2002] have noted that the limit of predictability is generally 7 days for synoptic scale weather systems and the associated high-impact weather occurring on smaller scales. The limits were attributed to initial state and data assimilation uncertainties, model uncertainties, and so-called "intrinsic uncertainties" that are unresolved in models.

Byerle and Paegle [2002, 2003] have explored the seasonal cycle and deviations from climatology around the Andes, Rockies and Tibetan plateau, focusing on the summer season. In the former two regions, low-level jet (LLJ) and precipitation responses occur east of the mountain ranges. These may be related to variations of ambient zonal flows interacting with orography during summer. The LLJ is a component of the mean, lower troposphere, eddy cyclonic circulation which persists around the Andes and Rockies during summer. A preliminary conclusion is that if anomalously strong and broad, upper level zonal flow exists over the orography, then the associated large inertia will promote predictability in all components, including the LLJ (e.g., the Great Plains LLJ) and precipitation, for a relatively long period.

The conclusion is based on 13 day, global ensemble forecasts during the summer, 1993, Mississippi River basin (MRB) floods and the extreme summer droughts over the region in the spring and early summer of 1988 [*Byerle and Paegle*, 2003]. Some basin scale representation of observed precipitation features is evident into the second week of the forecasts. This implies longer predictability of extreme summer events than some other prior studies.

It is now hypothesized that similar performance into the second week occurs in some winter cases of highly anomalous zonal flows over western North America. The large spatial structure and persistence of the selected anomalies may also contribute to improved forecasts [e.g., *Lorenz*, 1969].

This investigation analyzes two-week forecasts of precipitation and larger scale parameters for a small sampling of extreme events. Monthly averaged zonal flow anomalies over western North America are chosen a posteriori, and then composite two-week simulations are presented during the extreme (high and low wind) months. The results show that a global research model and MRF Reforecasts can successfully simulate the selected flows for almost 10 days. Persistence of the anomalies is discussed and anomaly correlations of persistence forecasts are presented.

Diagnostics from the NCEP/NCAR Reanalysis [*Kalnay et al.*, 1996; *Kistler et al.*, 2001] are introduced in section 2. Temporal correlations based upon a 50 year record suggest that January precipitation is more intense over western North America when the area averaged, upper troposphere, zonal flow is stronger than normal over that region. Subsequent sections explore the two-week forecasts during extremes in zonal flows over western North America.

Section 3 describes the models and experimental set up. Global model forecasts are selected a posteriori based upon weak and strong, upper troposphere, anomalous zonal flows impinging

upon the Rocky Mountains. Years of anomalously strong zonal winds are wetter over the region, while years with anomalously weak zonal winds are relatively drier. Simulations using four model configurations are examined: (1) the uniform resolution Utah Global Model (UGM) [*Paegle*, 1989], with wave number 42 truncation on 20 levels; (2) the NCEP Medium Range Forecast system (MRF) Reforecasts, available from the Climate Diagnostics Center [*Hamill et al.*, 2004], with wave number 62 truncation on 28 levels; (3) a rotated, variable resolution version of the UGM, which allows two-way interaction between an inner, 1° resolution region centered around the Rockies and an outer, 2° resolution global domain; and (4) a rotated, variable resolution "stretched" grid version of the UGM, which has a maxiumum of 0.5° resolution over the western U.S. The emphasis will be upon (1) and (2), above, the uniform resolution model configurations. Global simulations of the uniform resolution UGM, introduced in section 4, are able to delineate between the wet and dry regimes, and variable resolution approaches provide greater local detail.

Model precipitation forecasts are presented in section 5. Ratios of accumulated precipitation comparing strong zonal flow (wet) and weak zonal flow (dry) events are used to assess how well the models distinguish extreme precipitation events over the western U.S. Model forecasts are able to delineate qualitatively between the wet and dry conditions 5 and 10 days into the forecast.

Section 6 evaluates model skill for larger scales with anomaly correlations of 500-mb geopotential heights for the January cases. The MRF Reforecast case sampling is expanded by considering strong anomalous zonal flow (wet) events for December, January and February. The composites for each model exhibit greater skill than typically found in the second week of the forecasts. Section 7 provides further interpretation and discussion of the persistence of the anomalies, and Section 8 provides a summary and conclusions.

2. Deviations from Winter Climatology

The Rocky Mountain region has a pronounced reversal in the low level atmospheric circulation between summer and winter. A transition from a winter anticyclone to a summer cyclone has often been described in terms of thermal influences, such as "thermal low" in summer; or "cold-core anticyclone" and associated stagnant conditions in winter. *Peyrefitte* [1986] analyzed Great Basin surface anticyclones from 1962-1977. He found an anticyclone 64% of the time when snow cover over the plateau was 80% or more. He could not identify one instance during the 15 years when the plateau anticyclone persisted for more than three days with no snow cover. *Gutzler and Preston* [1997] examined winter snow cover as it related to summer convection over the Southwest and suggested a thermal explanation for the seasonal oscillations. They described surface heating in relation to dry and wet soils that occur in dry and snowy winters, respectively. *Byerle and Paegle* [2003] suggested an alternate explanation for the winter anticyclone and the winter-summer seasonal reversal in the circulation, emphasizing dynamical processes associated with changing zonal flows over the Rocky Mountains.

Fig. 1 displays the 700-mb eddy geopotential winds and heights using a seasonal average from 50 January and July months (1951-2000) from the NCEP/NCAR Reanalysis monthly archives. Eddies are defined by removing the zonal average in order to view the wave portion of the field. An anticyclonic circulation persists around the Rocky Mountains in the lower troposphere during January (Fig. 1a). The 200-mb eddy field (not shown) also includes an anticyclone over western North America during winter, whose center is displaced west of the 700-mb anticyclone. The westward tilt suggests the baroclinic nature of the midlatitude eddy anticyclone (not shown). The lower troposphere anticyclone is replaced by a trough in July (Fig. 1b), centered just off the west coast of California.

Fig. 2a shows the time correlation (1951-2000) during January between the area averaged, 200-mb zonal flow in the outlined box (30°-50°N, 130°-100°W) with 700-mb wind at all locations on the map. The eastward (northward) component of the vectors indicates the magnitude of the correlation coefficient between the area averaged, upper tropospheric wind in the box against the local zonal (meridional) flow component at 700 mb. Correlation coefficents of 0.3 are statistically significant with a 99% confidence level. The counterclockwise (cyclonic) orientation of the correlation vectors over western North America suggests that increased upper troposphere zonal flow over the mountains (given by the area average in the box) is associated with a weakened mean, 700-mb eddy anticyclone over the region.

Fig. 2b introduces a time correlation (1951-2000) between area averaged, 200-mb zonal flow in the same box with precipitation during January. The highest correlation coefficients are centered over the western U.S., suggesting a precipitation response that affects winter hydrology and snow pack generation over high terrain. The region of highest correlation (0.6) extends from northern California and southern Oregon to the Intermountain West.

Enhanced upper troposphere westerlies should tend to weaken the climatological winter anti-cyclone over western North America, and may lead to more transient storm tracks. Anomalously strong, zonally averaged winds may be promoted over the northeast Pacific Ocean and into western North America, for example, during warm, ENSO events. The correlations presented above are not particularly sensitive to whether the longitudinal extent of the box is over land or just off the west coast of North America. For example, results are similar if the westward extent of the box for the area average is confined more to the continent at 120°W-100°W.

3. Model Methodology

3.1 Experimental Set up

Global simulations are used to examine how ambient zonal flow anomalies may influence two-week forecasts during winter over western North America. January months characterized by anomalous, upper troposphere zonal flow impinging upon the Rocky Mountains were selected. A time series of January, area averaged, 200-mb westerly flow is depicted in Fig. 3 (1949-2000) from the NCEP/NCAR Reanalysis. The area average is taken over the region portrayed by the box in Fig. 2. The average, 200-mb zonal flow in the box during January for all years is 25.2 m/s (dashed line). Januaries with zonal flow exceeding the average by at least 1.2 standard deviations are referred to as "u200hi," and those for which the average zonal flow is at least 1.2 standard deviations below the average are referred to as "u200lo" cases. The strong flow years ("u200hi) have an area average 200-mb zonal flow of approximately 32 m/s, while the years of weaker zonal flow ("u200lo") average about 19 m/s. U200hi years are January 1950, 1952, 1969, 1996 and 2000; and u200lo years are January 1949, 1976, 1981, 1984, 1985 and 1992.

3.2 Uniform Resolution UGM and MRF Reforecasts

The uniform resolution UGM is initialized on 10 January at 00 UTC during each u200hi and u200lo year, and forecasts are made to 15 days (360 hours). The UGM is a multilevel, primitive equation version of the model described by *Paegle* [1989]. It has been used to address predictability questions [e.g., *Vukicevic and Paegle*, 1989; *Paegle et al.*, 1997; *Wang et al.*, 1999; *Miguez-Macho and Paegle*, 2001; and *Byerle and Paegle*, 2003]. The UGM is similar to global models used in most operational centers, the exception being its numerical treatment, which employs finite element methods in latitude and in the vertical and Fourier series in longitude. It

is hydrostatic, and predicts vorticity, divergence, thermal and moisture fields on pressure-based sigma coordinates. The uniform resolution model has 20 vertical levels, wave number 42 truncation in longitude and 2.2° latitude spacing. Model clouds are diagnosed in terms of relative humidity. The "emissivity" method is used for infrared radiative transfer (water vapor, carbon dioxide, clouds and the earth's surface are the only emitters and absorbers). Radiative processes include cloud-radiative interactions as described in *Nicolini et al.* [1993]. Convective and stratiform precipitation are parametrized similarly to methods used in the 1987 version of the NCAR Community Climate Model [*Bath et al.*, 1987].

The UGM does not contain a complete land parametrization. Initial surface temperature is specified globally from the reanalyses. Surface temperature in subsequent time steps is computed using a heat balance equation that includes short and longwave radiation, soil or water conduction and atmospheric turbulent and latent heat transfer. Initial conditions are 6-hourly NCEP/NCAR Reanalysis fields, except for latent heat flux, which is specified over the globe from the monthly-averaged Reanalysis climatology for January (1951-1999). The time step in the uniform resolution UGM is 900 seconds. Additional information regarding the current model configuration is outlined in *Byerle and Paegle* [2003].

The Climate Diagnostics Center has provided forecasts from the MRF Reforecast project [*Hamill*, 2003; *Hamill et al., 2004*]. Ensemble average and individual ensemble member forecasts are available with wave number 62 truncation, 28 levels in the vertical, and they have been initialized with NCEP/NCAR Reanalyses. Bred modes of 15 members comprise the ensemble average forecasts [*Toth and Kalnay*, 1997], and they are based upon NCEP's operational MRF model during January to June 1998 [*Caplan et al.*, 1997; *Wu et al.*, 1998]. The data are available through the worldwide web at cdc.noaa.gov/~jsw/refcst/, from 1979-2003. U200hi and u200lo (see section

3.1), 12 hour accumulated precipitation and 500-mb geopotential heights (every 24 hours) for the ensemble average forecasts initialized 10 January, 00 UTC were obtained. The January u200hi years within this time frame are 1996 and 2000 (Fig. 3). The u200hi MRF composite forecasts presented in sections 5 and 6 therefore represent an ensemble of 30 members (15 per year). The January u200lo years available are 1981, 1984, 1985 and 1992, representing 60 ensemble members.

The MRF sampling of strong and weak wind events is somewhat small and unbalanced, and is limited by the January cases that fall within the years of the MRF Reforecast project (1979-2003). The MRF sample is increased in section 6 (500-mb anomaly correlation evolution) by also considering strong zonal flow cases (same criteria described in section 3.1) occurring in December and February. MRF u200hi and u200lo ensembles are analogous to the definition of "ensemble" used for simulations of the summer 1988 droughts and 1993 floods [*Byerle and Paegle*, 2003]. That study employed a single version of the uniform resolution UGM, and was initialized with different global reanalyses (NCEP/NCAR and ECMWF) over one week during the respective drought and flood years.

The UGM can also be applied with variable resolution. This is done here by "telescoping" into the Rocky Mountain region as described in the appendix. The resulting forecasts provide better local resolution of orography and of precipitation. Variable resolution, however, may produce more truncation error at larger scales. The relative benefits/problems of this approach are discussed in relation to the selected events.

4. Uniform Resolution UGM Precipitation and Wind Verification

Results of the simplest forecasts are presented using the relatively low resolution version of the UGM. More advanced, variable resolution simulations with the UGM and ensemble forecasts from the MRF are briefly summarized in section 5 (see also the appendix).

Composites of precipitation accumulation are shown in Fig. 4. Fig. 4a depicts observed, 15 day precipitation totals averaged for years with significantly stronger than normal 200-mb zonal flow across the central Rocky Mountains (u200hi), and Fig. 4b presents averaged uniform resolution UGM forecasts for these cases. Observations are from the Climate Prediction Center's (CPC's) Unified data set of daily averaged precipitation over the continental U.S. [*Higgins et al.*, 1996], and consist of station observations interpolated to a 0.25° x 0.25° grid using a Cressman scheme. Measurable precipitation covers a large portion of the western U.S., including Washington, Oregon and California, with peaks greater than 30 cm over the Sierra Nevada Range (Fig. 4a). Precipitation is also oriented north-to-south across Idaho. Observations of the five-case, u200hi composite support the interannual signal of precipitation related to upper troposphere zonal flow over the region during January (Fig. 2b).

Fig. 5 shows 15 day observed and predicted precipitation accumulation from the uniform resolution UGM for the composites with anomalously weak upper troposphere zonal flow across the Rocky Mountains (u200lo). Accumulations during the u200lo years (Fig. 5a) are much smaller along the western coastal states (12 cm maximum over Washington), and the Intermountain West is dry compared to the u200hi composite (Fig. 4a). Average u200lo predicted precipitation accumulation is depicted in Fig. 5b. The forecast is much drier, with a peak over the U.S. less than half the maximum of the u200hi prediction. Model results are smoothed relative to observations, owing to the coarser model grid (2.8° longitude x 2.2°

latitude) compared to the CPC Unified grid (Figs. 4 and 5). The areal extent of accumulated precipitation is fairly representative in both sets of experiments, but peak magnitudes are underrepresented.

Time evolution of area averaged, accumulated precipitation for a box encompassing most of the western U.S. (124°-110°W, 34°-49°N) is displayed in Fig. 6. Observations (CPC Unified) show more than five times more precipitation for u200hi than for u200lo composites. The u200hi model ensemble curve closely matches observations for about 96 hours (4 days), then slightly under predicts accumulations to 216 hours (9 days). The model, area averaged precipitation for the winter u200hi composite does not significantly diverge from observations until about 240 hours (10 days) into the forecast. Around that time, model accumulations level off compared with observations, predicting about 83% of the observed accumulations by the 15-day point. Area averaged, u200lo observed precipitation accumulation is under 1.5 cm after 15 days (Fig. 6). The UGM over predicts the 15 day u200lo accumulation by about 40%. Model forecasts produce more than twice the precipitation in the u200hi simulations as in the u200lo ones at both 240 and 360 hours (10 and 15 days), suggesting they are able to distinguish between the relatively wet and dry extremes. An observed climatology for the two-week period beginning 10 January is also included in Fig. 6.

Byerle and Paegle [2003] examined medium range predictability over the Mississippi River Basin (MRB) during the summer 1993 floods and 1988 droughts using the UGM. During summer 1993, anomalously strong, upper troposphere zonal flow persisted over the central Rocky Mountains, while zonal flows were much weaker than normal during the spring and early summer droughts of 1988. They suggested that the large scale, ambient zonal flows interacting with Rocky Mountain orography may have a role in the circulation and hydrological features

over the MRB for those extreme events, particularly during the first week of two week forecasts (see their Fig. 16). The forecast ensembles were chosen based upon extreme wet and dry summers. The winter composites presented in this section are chosen based upon anomalous, upper troposphere zonal flows over the Rockies. In addition to the above components, the persistence of the high/low wind anomalies and associated circulation features may also play a role in the improved model performance. This is discussed further in section 7.

Fig. 7 shows the daily evolution of the area averaged, upper troposphere zonal wind for the uniform resolution UGM ensembles over the Rocky Mountain region (130°W-100°W, 30°N-50°N). The 200-mb zonal flow in the Reanalysis ranges between about 32 and 40 m/s for the u200hi cases. It is weaker in the u200lo cases, between approximately 16 and 21 m/s. The UGM ensemble forecasts are fairly representative of the reanalyzed, upper troposphere zonal flows during the 15 days. For the u200hi ensemble, the UGM zonal flow at sigma level 0.22 closely resembles 200 mb in the Reanalysis between days 9 and 11. The u200hi, area averaged, precipitation accumulation is also representative at 10 days, under predicting observations by about 0.4 cm (Fig. 6). The next section addresses the precipitation forecasts of other model configurations over the western U.S. and examines the extent to which they delineate between wet and dry events.

5. Comparison of Precipitation Forecasts

Precipitation accumulation and wind verification for the uniform resolution UGM (section 4) suggest some usefulness in the forecasts into the second week. This section assesses the extent to which the UGM and MRF Reforecasts are able to delineate between the u200hi and u200lo precipitation (section 5.1). Maps of 10 day accumulations are also presented (section 5.1).

5.1 Area Averaged Accumulations

A ratio of accumulated precipitation between u200hi and u200lo composites is presented for the western U.S. and several subregions. Fig. 8 shows the regions over which the area averaged precipitation is calculated. Area I is a broad region of the West (Fig. 8a). It corresponds to the area average for which precipitation is calculated for the uniform resolution UGM in Fig. 6. Additional regions are depicted in Fig. 8b (II: northern states; III: California, Nevada; IV: Colorado basin). Along with I-IV, precipitation ratios for the combined area average of locations III and IV are also presented. Ratios of accumulated precipitation are presented in Tables 1-5.

Table 1 shows the ratio of u200hi to u200lo precipitation accumulation at days 5, 10 and 15 over region I of Fig. 8 (western U.S.). The first two models listed have uniform resolution ("Uniform UGM" and "MRF Reforecast"), and the other two are variable resolution UGM configurations with higher local grid spacing ("UGM two-way grid" and "UGM Stretched grid"). Observed, CPC Unified precipitation ratios are in parentheses. Observed ratios of the MRF Reforecasts are different from the other three models because the former are a subset of the years comprising the 52 year time series (Fig. 3). They are limited by the u200hi and u200lo cases falling between 1979-2003 (two u200hi and four u200lo cases).

Over region I (Table 1), all models produce ratios greater than 2 at day 5, suggesting they differentiate between the observed wet and dry extremes. The MRF Reforecast ratio is the lowest (2.6 compared to 4.9 observed). By day 15, the models' ability to distinguish between wet and dry events is clearly degraded. Only the uniform resolution UGM has a ratio above 2. Similar conclusions hold for the sub-basins and are summarized in the tables mentioned above.

Overall, the data suggest that most of the model configurations, particularly those of the UGM, delineate qualitatively between u200hi and u200lo precipitation at days 5 and 10. The

uniform resolution UGM consistently has ratios at or above 2 when observed ratios are above 2, even on day 15. However, the poor performance of the other model forecasts suggests that 15 day results are not generally useful, and that the relatively good skill of the uniform resolution UGM at 15 days may be an artifact of the small sample.

5.2 Precipitation Maps

Composites of accumulated, 10 day precipitation are presented for each u200hi and u200lo model configuration. Observations are from the CPC Unified data set [*Higgins et al.*, 1996] as in sections 4 and 5.1.

Fig. 9 displays u200hi precipitation accumulations corresponding to the composites available during the years of the MRF Reforecast project (1979-2003). Observations (Fig. 9a) show a maximum near 22 cm along the Oregon-California border, and another near 14 cm is over the Sierra Nevada range. The MRF Reforecast has a grid spacing 10 times as large as the observations. It depicts the general signature of the observations, with precipitation covering a broad area (Fig. 9b). The MRF misses details over the coastal states, and does not clearly distinguish between areas of precipitation to the east. Similar to the MRF, the UGM (also the average of just the 1996 and 2000 u200hi cases) has a maximum accumulation over California and Oregon (Fig. 9c).

U200lo composites corresponding to MRF Reforecast years are depicted in Fig. 10. The maximum observed accumulation over the West (Fig. 10a) is about 20% of the u200hi composite (Fig. 9a). The MRF produces more area averaged, u200lo precipitation than do both the uniform and variable resolution UGMs during the second week (e.g., at day 10). The uniform resolution, u200lo UGM composite produces a broad area of 1-2 cm accumulation at day 10 (Fig. 10c).

Figs. 9 and 10 show composites for the u200hi and u200lo cases between 1979-2003. Figs. 11 and 12 show similar maps of u200hi and u200lo observations and UGM configurations covering the 52 years (1949-2000). While areal coverage of uniform resolution UGM precipitation is broader than observed (Fig. 11a,b and 12a,b), variable resolution forecasts produce more detailed spatial structure (Fig. 11c,d and 12c,d). Areal coverage and magnitude, however, are generally lower in the variable resolution forecasts.

All model forecasts over predict u200lo precipitation accumulation at day 10. As an example, the "stretched" model predicts almost twice the amount of observed precipitation near the western border of Idaho (compare Fig. 12a and 12d). Area averaged amounts tend to be on the order of half the amounts in the u200hi composites (section 5.1), similar to that shown for the uniform resolution UGM (Fig. 6).

6. Forecast Validation of Height Field

Precipitation validation emphasizes forecast skill on relatively smaller spatial scales. It is instructive to consider geopotential height prediction which emphasizes larger scales and is generally evaluated in terms of anomaly correlations. Anomaly correlations were computed over the Northern Hemisphere (NH) (20°N-90°N), and locally, over western North America, including the central Rocky Mountains (30°N-60°N, 130°W-100°W), each without bias correction. Anomaly correlations for the forecast variable Z are calculated as:

$$\frac{\overline{(Z-Z_{cl})(Z_{ob}-Z_{cl})}}{\left[\overline{(Z-Z_{cl})^2}\,\overline{(Z_{ob}-Z_{cl})^2}\right]^{1/2}} \qquad (1)$$

where Zcl represents the climatological value of Z, and Zob is the observed value. The bars represents area averages of the variables. Climatology is defined by the 50 year, January average (1951-2000) from the NCEP/NCAR Reanalysis. "Observations" are also defined using the Reanalysis. Anomaly correlations of persistence forecasts, discussed in section 7, are computed by replacing forecast variable Z in equation (1) with the initial state variable.

Fig. 13 displays 500-mb anomaly correlations for the uniform resolution UGM. The sigma level output has been interpolated to pressure coordinates, and Reanalyses have been bilinearly interpolated to a 2.8° longitude x 2.2° latitude grid to match the model resolution. This accounts for correlation coefficients below 1.0 at the initial hour. Fig. 13a shows composites of the 11 cases (u200hi and u200lo) described in section 3.1. The UGM maintains useful skill (generally considered at or above 0.6) over the NH for almost 144 hours (6 days) into the forecast. Over the Rocky Mountain region, the composite anomaly correlation for all cases maintains a value at or above 0.6 longer into the forecast relative to the NH (Fig. 13a). The curve is similar to the zonally averaged curve for all cases during the first 108 hours (4.5 days). Subsequently, the local curve climbs to just under 0.7 at the 168 hour (7 day) point and remains above 0.6 until 180 hours (7.5 days). When the individual u200hi and u200lo composites were considered separately, uniform resolution UGM u200hi composites performed better, both over the NH and western North America.

The u200hi (wet) cases tend to be of greater societal importance for these time scales. The u200hi composite anomaly correlation is illustrated in Fig. 13b. Useful forecast skill for the NH zonal average is maintained to just beyond 144 hours (6 days), approximately 7 hours longer than for the 11 case average (compare Fig. 13a and Fig. 13b), and about 12 hours longer compared to the u200lo composite (not shown). The anomaly correlation over the Rockies region

is significantly larger beyond 108 hours (4.5 days), and does not fall below 0.6 until 228 hours (9.5 days) into the forecast. Local predictive skill for 500-mb heights is maintained for about 3.5 additional days compared to the entire NH.

Anomaly correlations are also computed for u200hi years corresponding to the MRF Reforecast project (1979-2003) (Fig. 14). The sampling of January cases between 1979-2003 is small, particularly for the u200hi cases (only 1996 and 2000). To extend the winter sample, corresponding anomalies for December and February are selected using the same criteria for January (see section 3.1). A December-January-February (DJF) average is shown in Fig. 14. The composite now consists of 10 independent, u200hi forecasts initialized on the 10th day of the month. As with the UGM, "observations" and climatology for the correlations are from the NCEP/NCAR Reanalysis. The monthly averaged, climatological 500-mb geopotential height (1951-2000) corresponding to the month of the forecast is used. For example, anomaly correlations for December forecasts use December climatology (Fig. 14).

The composite MRF correlation over the NH remains above 0.6 for about 204 hours (8.5 days) (Fig. 14a). The MRF Reforecast anomaly correlation for climatology is also included, based upon forecasts initialized on 10 December, January and February, from 1979-2003 (the average of 75 forecasts). The NH u200hi composite maintains forecast skill for about 18 hours longer than that of climatology.

The composite MRF correlation for the Rockies region (Fig. 14b) remains above 0.6 for about 228 hours (9.5 days), similar to the five-case UGM January composite (Fig. 13b). Climatology shows useful forecast skill over western North America to approximately 168 hours (7 days) (Fig. 14b).

Anomaly correlations of the composite u200hi and u200lo, variable resolution forecasts are shown in Fig. 15. NCEP/NCAR Reanalysis "observations" and climatology have been interpolated to the same uniform grid spacing as model output (1°) to compute the anomaly correlations. Fig. 15a depicts curves for the two-way nested model, which has a 1° resolution polar cap north of the 44°N latitude circle. Fig. 15b shows the composite for the stretched model. Correlations of the uniform resolution UGM are included in both panels for comparison. Variable and uniform resolution curves closely match each other through the first 96 hours (4 days) of prediction (Fig. 15a and Fig. 15b). Some loss of skill in the variable resolution forecasts is noticeable beyond 4 days. The stretched model curve is briefly superior to the uniform resolution UGM around the Rocky Mountain region near 168 hours (1 week) (Fig. 15b).

7. Discussion

The larger scale characteristics of cold season events have been found to contribute to overall greater forecast skill of extreme winter precipitation events [*Olson et al.*, 1995]. *Gartner et al.* [1996] suggested that understanding the role of topography in organizing precipitation is more difficult. They noted that for the continental U.S., the highest equitable threat scores of the meso-Eta were around the West coast, which is just downstream of the data sparse Pacific. The orographic organization of precipitation around the West Coast may partially account for the improved predictability. However, the same explanation did not apply to portions of the central and eastern Rocky Mountains, where the skill scores of the Eta model were relatively low [*Gartner et al.*, 1996].

Two-week January forecasts have been analyzed based upon extremes of upper troposphere zonal flow over the Rocky Mountain region. Ratios of area averaged u200hi (wet) to u200lo (dry) precipitation accumulation over the western U.S. and various sub-basins illustrate some of the

challenges on these time scales (Tables 1-5). Over the Colorado River basin, for example (region IV of Fig. 8), ratios are too high at day 5, suggesting higher potential for false alarm forecasts of wet events (Table 5). Over California and western Nevada, the variable resolution forecasts delineate best between wet and dry events at day 5 (Table 4).

The composite, uniform resolution UGM maintains a 500-mb geopotential height anomaly correlation at or above 0.6 over the NH for 6 days in these extreme events (Fig. 13a), approximately 1.5 days longer than usually found with the same model during winter [*Miguez-Macho and Paegle*, 2000; and *Roman et al.*, 2004]. Useful anomaly correlation of the MRF geopotential height field over the NH for the composite u200hi (1996 and 2000) and u200lo (1981, 1984, 1985 and 1992) cases in January extends to 9.5 days (not shown). We should emphasize the distinction between the UGM composites (research model, single forecasts) and the MRF composites, which consist of state-of-the-art, operational model averages of ensemble means (15 members).

In u200hi cases, the large inertia associated with a persistent and strong background zonal flow, both upstream and over the central Rockies, may contribute to a relatively longer forecast signal (see Fig. 13b and Fig. 14b). In the uniform resolution UGM, local predictability of 500-mb heights is maintained approximately 3.5 additional days compared with the NH (Fig. 13b). Previous studies [e.g., *Mo et al.*, 1995] have suggested that anomalous zonal flows interacting with orography may have contributed to extreme summer flooding of the Mississippi River basin (MRB) during summer 1993 and that the flow anomalies may have contributed to extended predictability over the MRB [*Byerle and Paegle*, 2003]. Forecasts of both the u200hi and u200lo winter composites perform relatively well for 500-mb geopotential height correlations. For example, a composite (9 cases) of u200lo, MRF winter forecasts (DJF, similar to Fig. 14a but for

u200lo), does not fall below 0.6 for the NH until 9 days (not shown). Higher anomaly correlations may imply persistence of the anomalies. Large scales of the anomalies and their persistence may therefore promote longer predictability, even if the regional inertia is small.

Lorenz [1969] demonstrates that larger scales possess longer predictability. We speculate that both u200hi and u200lo cases are characterized by large scale anomaly fields whose associated persistence may promote a longer forecast signal.

Support of this conjecture is illustrated in Fig. 16, which shows the the composite, monthly averaged, 500-mb geopotential fields for the cases of strong and weak zonal flow across the Rocky Mountains (NCEP/NCAR Reanalysis). In u200hi cases, the geopotential height field has low amplitude over western North America with near-zonal westerly flow (Fig. 16a). An anticyclonic circulation is located over the North Pacific Ocean near the Aleutian Islands. By contrast, the 500-mb geopotential height field for the u200lo composite (Fig. 16c) shows an anticyclonic circulation located over western North America, more typical of the January climatology (e.g., compare to Fig. 1a). The wave pattern for the two composites is illustrated by subtracting the 50-year January climatology from each composite. In cases of strong zonal flow across the Rockies, a 120 m anomaly is located over the North Pacific Ocean and anomalously lower heights are over western North America (Fig. 16b). The dry (u200lo) cases display a reversal of the circulation over the Rocky Mountains and upstream over the Pacific Ocean in comparison to the wet (u200hi) cases (Fig. 16d). The former (u200lo) is characterized by synoptic patterns broadly resembling the Pacific North America (PNA) pattern [*Horel and Wallace*, 1981]. The reversals between u200hi and u200lo are also somewhat reminiscent of superresonant and subresonant orographic responses studied by *Charney and Devore* [1979] and by *Nogués-Paegle* [1979]. The hypothesis that these large scale anomalies may promote

predictability is supported by the capacity of the simplest experiments using the uniform resolution UGM (section 4). Those experiments provide competitive 10 day skill over large regions of western North America.

The persistence of the chosen anomalies may also contribute to the improved model performance described in sections 4-6. The PNA pattern, for example, is generally persistent with time scales longer than just a few days [*Horel and Wallace*, 1981]. Such a pattern may hypothetically contribute to persistence and longer forecast skill in u200lo cases, which broadly resemble the PNA (Fig. 16d). To distinguish whether the models sustain persistence, 500-mb geopotential height anomaly correlations of persistence forecasts are shown in Figs. 13 and 14. Anomaly correlations of persistence fall below 0.6 during the first 48-60 hours (2-2.5 days) in Fig. 13a. Similar results are found in the MRF composites (Fig. 14a and b). In the five-case u200hi, UGM composite for the Rockies region (Fig. 13b), persistence (curve with boxes) maintains a higher value, with a correlation above 0.6 for about 150 hours (6 days, 6 hours). However, the persistence curve for the Rockies lags that of the model curve by about 3 days (Fig. 13b).

NH anomaly correlations in both sets of variable resolution experiments are slightly higher than the uniform resolution UGM during the first 72 hours (3 days) (Fig. 15). Some degradation of the forecasts was anticipated owing to larger formal truncation error in the variable resolution models compared to the fourth order truncation error of uniform resolution. Evidence of this is found over the Rockies region, where the variable resolution curves have fallen below the uniform resolution UGM curves at 120 hours (5 days). NH curves also remain slightly behind the uniform resolution composites from hour 120 (day 5) through most of the second week.

The overall similarity of the variable resolution correlations to those of the uniform resolution UGM is favorable given the lower formal accuracy in the variable resolution models and possible numerical irregularities in the two-way nested model (e.g., the abrupt transition from the 1° polar cap to the 2° outer grid). Examination of the 500-mb error fields (not shown) suggests that there are no irregularities around the regions of the rotated pole or the regions of abrupt change in resolution, and the higher local resolution produces more realistic precipitation patterns even though the higher resolution does not provide systematically better 500-mb anomaly correlation. Similar tests examining a rotated, global variable resolution set-up have been documented by Coté et al. (1998b). Their method rotates the mathematical poles away from the inner nest, producing a more isotropic subregion of resolution in both horizontal directions. They find "acceptably small" differences between rotated and uniform simulations over and around the inner domain at the 48 hour point (see their Fig. 7).

8. Summary and Conclusions

Simmons and Hollingsworth [2002] demonstrate that global models have exhibited substantial improvement in forecast accuracy during the past decade, with useful predictability extending to 1 week (their Fig. 4). A THORPEX science question asks, "[What are the] limits of predictability, and what determines these limitations [*Shapiro et al.*, 2003]?" THORPEX will explore methods that may mitigate these limitations, including the important use of ensemble prediction systems [*Shapiro et al.*, 2003]. The goal of this study has been to address medium range winter predictability enhancement over western North America using ensembles of global model forecasts chosen based upon a small number of extreme events.

A premise of our hypothesis for enhanced predictability is the interaction of Rocky Mountain orography with the ambient, upper troposphere, zonal flow. We explored anomaly correlations of 500-mb geopotential heights. Over the NH and the Rocky Mountain region, forecasts during the extreme events exhibit higher skill than typical of the UGM and MRF. The variable resolution UGM models also perform at least as well as, or better than the uniform resolution UGM during the first 4 days of prediction. The number of cases sampled was small. The case sampling was increased for the MRF Reforecasts to evaluate anomaly correlations for all winter months (DJF). Useful skill (0.6) for some cases extends to 9.5 days in the uniform resolution composites (Figs. 13b and 14b). Improved performance may be related to persistent, large inertia of the flow in wet events, and to increased predictability of initial, large scale anomalies in both wet and dry events [*Lorenz*, 1969].

Challenges to orographic precipitation forecasting over the complex terrain of the western U.S. have been highlighted by *Smith et al.* [1997], who identified areas of high research priority for the U.S. Weather Research Program (USWRP). One of their recommendations was that, "The question of deterministic predictability of topographically organized weather has special relevance in the case of precipitation and should be systematically examined."

We investigated the abilities of global model configurations to simulate precipitation over western North America during winter cases of anomalous, upper troposphere zonal flow over the region. Model forecasts delineate qualitatively between wet and dry events at both 5 and 10 days. They also exhibit regional strengths and weaknesses, as summarized in section 5.2, but 15 day predictions are generally not useful for these cases.

The uniform resolution model forecasts maintain representative precipitation to about 10 days over the western U.S. (e.g., Fig. 6). Horizontal maps of 10 day accumulation suggest more

detail in the UGM variable resolution forecasts, particularly in the "stretched" model. The stretched model composite of u200hi events differentiates between three of the observed regions of precipitation (Fig. 11). However, it is possible that similar detail would result if the cruder, uniform UGM output were statistically downscaled in post processing. This has not yet been explored.

We selected forecasts based upon previous knowledge of the upper troposphere zonal flow anomalies over western North America. Monthly averaged conditions and deviations from the climatology show a significant correlation between area averaged, upper troposphere zonal flow over the central Rocky Mountains and precipitation over the region (section 2). The diagnostics and model experiments suggest that flow modifications associated with ambient flows exist over the orography during the winter season, and that in such cases a predictable regional response may be present to about 10 days. We have diagnosed two-week forecasts for a small sample of extreme cases, and present conclusions are therefore limited by the small sampling. A question for further examination is whether the extended predictability applies only to the extreme, chosen events; or whether systematic forecasts of opportunity may be possible without prior information about monthly averaged anomalies.

Appendix: Rotated, Variable Resolution UGM

Topographic representation should be improved to increase accuracy of precipitation forecasts. This may be accomplished with the UGM by applying rotated, variable resolution, as outlined in Fig. A1a. Fig. A1a shows the uniform resolution grid in the usual spherical coordinate. It depicts the same grid that is used for the uniform resolution UGM cases, with 129

points in longitude and 82 points in latitude. Contours of topography represent the Rocky Mountains as a broad massif, with peaks under 2500 m.

The rotated approach takes advantage of the convergence of the meridians and therefore closer spacing between grid points near the polar regions. Higher local resolution benefits from reduced horizontal diffusion, which is proportional to the latitudinal grid spacing. The configuration is similar to two-way nested grid techniques available in other models in which resolution changes abruptly. For example, Coté et al. (1998a,b) employ a rotated, variable resolution model for application to a broad range of time scales. Unlike the method applied here, the mathematical poles are rotated away from the high resolution inner domain

The mathematical pole is rotated to 40°N, 110°W over northeastern Utah (Fig. A1b). The total number of latitude grid points is increased to 115, with longitudinal points remaining unchanged. The vertical grid contains 23 levels. Higher resolution near the mathematical north pole is obtained by increasing the concentration of latitudinal grid points north of 44°N while decreasing the resolution to the south (Fig. A1b). The first set of variable resolution experiments applies equally spaced, 2° latitude increments from the south pole, northward to 44°N, as in Fig. A1b. Resolution is increased to uniformly spaced, 1° latitude increments from 44°N to the north pole. Representation of the Rocky Mountains is improved, with peaks above 3000 m over Colorado. The Wasatch Mountains and Wind River range are delineated, as well as the Sierra Nevada range (Fig. A1b). This set of experiments is referred to as "two-way nested" runs.

A second rotated, variable resolution configuration employs a stretched grid approach (Fig. A1c), and is referred to as the "stretched" model. Resolution in latitude is 0.5° at the rotated north pole, located over Utah, as before (40°N, 110°W). Latitudinal grid spacing increases gradually by 1% with each grid point from north to south. The configuration also has 129 points in longitude,

but latitudinal points have been increased to 152. The grid spacing gradually increases southward, so that the spacing at the rotated south pole is 2.3°. Topographical representation (Fig. A1c) is improved (compare to Figs. A1a and A1b). As examples, the Uinta Mountains east of the Great Salt Lake appear, as well as some of the other principal ridge heights of the Rockies. The Sierra Nevada Range becomes more clearly resolved over California.

The time step for the variable resolution simulations is 400 seconds, and integrations are run to 15 days. The model is initialized with NCEP/NCAR Reanalyses, as in the uniform resolution UGM experiments and the MRF Reforecasts. Graphical representation of model output requires interpolation to a uniform resolution grid. For each of the variable resolution approaches outlined above, global output is interpolated to a uniform, 1° grid.

Acknowledgments. This research was supported by NSF grants ATM0106776, ATM0109241 and NOAA/PACS grant NA030AR4310094 to the University of Utah. The USAF has provided support to the first author; and the views expressed are those of the author and do not reflect the official policy or position of the United States Air Force, Department of Defense, or the U.S. Government. We have benefitted from discussions with J. Nogués-Paegle. We thank the Climate Diagnostics Center for developing and facilitating the use of the MRF Reforecasts. We also acknowledge the maintainers of the NOAA Operational Model Archive and Distribution System (NOMADS) data portal for making available portions of the NCEP/NCAR Reanalysis used in this study, and also to members of the Center for Ocean-Land-Atmosphere Studies (COLA) who continually facilitate access to the data through the GRADS-DODS server. Finally, we express sincere appreciation to anonymous reviewers for comments and suggestions which have improved this research and the manuscript.

References

Bath, L. M., M. A. Dias, D. L. Williamson, G. S. Williamson, and R. J. Wolski, User's Guide to NCAR CCM1, Technical Report NCAR/TN-286+IA, National Center for Atmospheric Research, 173 pp., 1987.

Byerle, L. A., and J. Paegle, 2002, Description of the seasonal cycle of low-level flows flanking the Andes and their interannual variability, *Meteorologica*, *27*, 71-88, 2002.

Byerle, L. A., and J. Paegle, Modulation of the Great Plains low-level jet and moisture transports by orography and large-scale circulations, *J. Geophys. Res.*, *108*(D16), 8611, doi:10.1029/ 2002JD003005, 2003.

Caplan, P., J. Derber, W. Gemmill, S.-Y. Hong, H.-L. Pan, and D. Parrish, Changes to the 1995 NCEP operational Medium-Range Forecast Model analysis-forecast system, *Wea. Forecasting*, *12*, 581-594, 1997.

Charney, J. G., and J. Devore, Multiple flow equilibria in the atmosphere and blocking, J. *Atmos. Sci.*, *36*, 1205-1216, 1979.

Chen, M., P. Xie, J. E. Janowiak, and P. A. Arkin, Global land precipitation: a 50-year monthly analysis based on gauge observations, *J. Hydrometeorol.*, *3*, 249-266, 2002.

Coté, J., S. Gravel, A. Methot, A. Patoine, M. Roch, and A. Staniforth, The Operational CMC-MRB Global Environmental Multiscale (GEM) Model. Part I: design considerations and formulation, *Mon. Wea. Rev.*, *126*, 1373-1395, 1998a.

_____, J.-G. Desmarais, S. Gravel, A. Methot, A. Patoine, M. Roch, and A. Staniforth, The Operational CMC-MRB Global Environmental Multiscale (GEM) Model. Part II: results, *Mon. Wea. Rev.*, *126*, 1397-1418, 1998b.

Fritsch, J. M., R. A. Houze, Jr., R. Adler, H. Bluestein, L. Bosart, J. Brown, F. Carr, C. Davis, R. H. Johnson, N. Junker, Y.-H. Kuo, S. Rutledge, J. Smith, Z. Toth, J. W. Wilson, E. Zipser, and D. Zrnic, Quantitative precipitation forecasting: report of the eighth prospectus development team, U.S. Weather Research Program, *Bull. Am. Meteorol. Soc.*, *79*, 285-299, 1998.

Gartner, W. E., M. E. Baldwin, and N. W. Junker, Regional analysis of quantitative precipitation forecasts from NCEP's "early" Eta and meso-Eta models, Preprint volume, 16 Conference of the American Meteorological Society on Weather and Forecasting, Norfolk, VA, 187-189, 1996.

Gutzler, D. S., and J. W. Preston, Evidence for a relationship between spring snow cover in North America and summer rainfall in New Mexico, *Geophys. Res. Lett.*, *24*, 2207-2210, 1997.

Hamill, T. M., Evaluating forecasters' rules of thumb: a study of d(prog)/dt, *Wea. Forecasting, 18*, 933-937, 2003.

____, J. S. Whitaker, and X. Wei, Ensemble re-forecasting: improving medium-range forecast skill using retrospective forecasts, *Mon. Wea. Rev., in press*, 2004.

Higgins, R. W., Y. Yao, J. E. Janowiak, and Y. P. Yao, A gridded hourly precipitation data base for the United States (1963-1993), NCEP/Climate Prediction Center, Atlas 1, NCEP/Climate Prediction Center, Camp Springs, MD, 1996.

Horel, J. D., and J. M. Wallace, Planetary-scale atmospheric phenomena associated with the Southern Oscillation, *Mon. Wea. Rev., 109*, 813-829, 1981.

Kalnay, E., M. Kanamitsu, R. Kistler, W. Collins, D. Deavan, L. Gandin, M. Iredell, S. Saha, G. White, J. Woollen, Y. Zhu, M. Chelliah, W. Ebisuzaki, W. Higgins, J. Janowiak, K. C. Mo, C. Ropelewski, J. Wang, A. Leetma, R. Reynolds, R. Jenne, and D. Joseph, The NCEP/NCAR 40-year reanalysis project, *Bull. Am. Meteorol. Soc., 77*, 437-471, 1996.

Kistler, R., E. Kalnay, W. Collins, S. Saha, G. White, J. Woollen, M. Chelliah, W. Ebisuzaki, M. Kanamitsu, V. Kousky, H. Dool, R. Jenne, and M. Fiorino, The NCEP-NCAR 50-year reanalysis: monthly means cd-rom and documentation, *Bull. Am. Meteorol. Soc.*, 82, 247-268, 2001.

Lorenz, E. N., The predictability of a flow which possesses many scales of motion, *Tellus, 21*, 289-307, 1969.

Miguez-Macho, G., and J. Paegle, Sensitivity of a global forecast model to initializations with reanalysis datasets, *Mon. Wea. Rev., 128*, 3879-3889, 2000.

Mo, K. C., J. N. Paegle, and J. Paegle, Physical mechanisms of the 1993 summer floods, *J. Atmos. Sci., 52*, 879-895, 1995.

Nogués-Paegle, J., The effect of topography on a Rossby wave, *J. Atmos. Sci., 36*, 2267-2271, 1979.

Olson, D. A., N. W. Junker, and B. Korty, Evaluation of 33 years of quantitative precipitation forecasting at NMC, *Wea. Forecasting, 10*, 498-511, 1995.

Paegle, J., A variable resolution global model based upon Fourier and finite element representation, *Mon. Wea. Rev., 117*, 583-606, 1989.

Peyrefitte, A. G., The plateau anticyclone of the western United States, Doctoral dissertation, Department of Meteorology, University of Utah, 123 pp., 1986.

Roman, J. C., G. Miguez-Macho, L. A. Byerle, and J. Paegle, Intercomparison of global research and operational forecasts, *Wea. Forecasting, 19*, 534-551, 2004.

Schultz, D. M., W. J. Steenburgh, R. J. Trapp, J. Horel, D. E. Kingsmill, L. B. Dunn, W. D. Rust, L. Cheng, A. Bansemer, J. Cox, J. Daugherty, D. P. Jorgensen, J. Meitin, L. Showell, B. F. Smull, K. Tarp, and M. Trainor, Understanding Utah winter storms: the Intermountain Precipitation Experiment, *Bull. Am. Meteorol. Soc., 83*, 189-21, 2002.

Shapiro, M. A., A. J. Thorpe, B. Atlas, D. Carlson, W. Dabberdt, A. Frolov, R. Gelaro, N. Gustafsson, P. Houtekamer, S. Jones, R. Langland, A. Lorenc, M. Morgan, R. Morss, T. Nakasawa, T. E. Nordeng, H. Olafsson, T. Palmer, H.-L. Pan, F. Rabier, R. Rotunno, P. Sardeshmukh, B. Smith, L. Smith, C. Snyder, Z. Toth, C. Velden, V. Wulfmeyer, and T. Xu, THORPEX international science plan, Version 2, *http://www.mmm.ucar.edu/uswrp/programs/thorpex.html*, 2003.

Simmons, A. J., and A. Hollingsworth, Some aspects of the improvement in skill of numerical weather prediction, *Quart. J. Roy. Meteor. Soc., 128*, 647-677, 2002.

Smith, R., J. Paegle, T. Clark, W. Cotton, D. Durran, G. Forbes, J. Marwitz, C. Mass, J. McGinley, H.-L. Pan, and M. Ralph, Local and remote effects of mountains on weather: research needs and opportunities, *Bull. Am. Meteorol. Soc., 78*, 877-892, 1997.

Stoelinga, M. T., P. V. Hobbs, C. F. Mass, J. D. Locatelli, B. A. Colle, R. A. Houze, Jr., A. L. Rangno, N. A. Bond, B. F. Smull, R. M. Rasmussen, G. Thompson, and B. R. Colman, Improvement of microphysical parametrization through observational verification experiment, *Bull. Am. Meteorol. Soc., 84*, 1807-1826, 2003.

Toth, Z., and E. Kalnay, Ensemble forecasting at NCEP and the breeding method, *Mon. Wea. Rev., 125*, 3297-3319, 1997.

Wang, M., J. Paegle, and S. P. Desordi, Global variable resolution simulations of Mississippi River basin rains of summer 1993, *J. Geophys. Res., 104*, 19399-19414, 1999.

White, B. G., J. Paegle, W. J. Steenburgh, J. D. Horel, R. T. Swanson, L. K. Cook, D. J. Onton, and J. G. Miles, Short-term forecast validation of six models, *Wea. Forecasting, 14*, 84-108, 1999.

Wu, W.-S., M. Iredell, S. Saha, and P. Caplan, Changes to the 1997 NCEP operational MRF model analysis/forecast system, National Centers for Environmental Prediction Technical Procedures Bulletin 443, National Weather Service, Office of Meteorology, Programs and Plans Division, Silver Spring, MD, 20910, 1997.

Figure captions

Fig. 1. Climatology of 700-mb eddy heights (m) and wind vectors (m/s) over North America for (a) January; and (b) July from the NCEP/NCAR Reanalysis monthly archive. Eddies are defined by removing the zonal average.

Fig. 2. Time correlation over North America (1951-2000) during January. (a) Correlation vectors of the area-averaged, 200-mb zonal wind in the outlined box (30°N-50°N, 130°W-100°W) with 700-mb wind at all locations. (b) Similar to (a), but 200-mb, zonal wind in the outlined box is correlated with precipitation over land (PREC/L of *Chen et al.*, 2002). The magnitude of correlation vectors is indicated at the bottom of panel (a), and only coefficients meeting the 99% statistical significance criteria (0.3) are plotted. Positive correlation coefficients greater than 0.3 are shaded in (b).

Fig. 3. Climatology of the area averaged, 200-mb zonal flow over western North America during January (30°N-50°N, 130°W-100°W), 1949-2000. The dashed horizontal line indicates the 52 year mean (25.2 m/s). Solid lines are drawn to indicate plus and minus 1.2 times the standard deviation from the mean.

Fig. 4. Average precipitation accumulation for the five u200hi composites (cm). (a) Observed, 15 day accumulation (10-24 January 1950, 1952, 1969, 1996 and 2000). (b) 15 day accumulation of the uniform resolution UGM. The contour interval is 2 cm in (a) and (b) (contouring in (a) is up to 20 cm). Shading is for accumulation greater than or equal to 3 cm. The maximum observed accumulation in (a) is 33 cm.

Fig. 5. Average precipitation accumulation for the six u200lo composites (cm). (a) Observed, 15 day accumulation (10-24 January 1949, 1976, 1981, 1984, 1985 and 1992). (b) 15 day accumulation of the uniform resolution UGM. The contour interval is 1 cm in (a) and (b). Shading is for accumulation greater than or equal to 3 cm.

Fig. 6. Composite u200hi and u200lo, area averaged precipitation accumulation (cm) (124°W-110°W, 34°N-49°N) from observations and the uniform resolution UGM. Time 0 is on 10 January. Observations are from the CPC Unified data set [*Higgins et al.*, 1996]. The line labelled with (+) marks indicates the 30 year CPC climatology of 10-24 January precipitation accumulation over the same region from 1970-2000 (excluding 1973).

Fig. 7. Composite u200hi and u200lo, area averaged, upper troposphere zonal wind (m/s) (130°W-100°W, 30°N-50°N) from the NCEP/NCAR Reanalysis and the uniform resolution UGM. The 200-mb zonal flow is plotted for the NCEP/NCAR Reanalysis, and the sigma level 0.22 zonal flow is plotted for the uniform resolution UGM.

Fig. 8. Regions over which the area average precipitation accumulation is calculated for model forecast comparisons. (a) Region I (western U.S.); (b) region II (northern states); (c) region III (California, Nevada); and (d) region IV (Colorado River basin).

Fig. 9. Composite of average day 10 precipitation accumulation (cm) of u200hi years (1996 and 2000). (a) Observed u200hi precipitation (Higgins et al., 1996). (b) MRF u200hi precipitation. (c) Uniform resolution UGM, u200hi precipitation. The contour interval is 2 cm (contouring in (a) is

up to 20 cm), and shading is for accumulation greater than or equal to 3 cm. The maximum observed accumulation in (a) is 24 cm.

Fig. 10. Composite of average day 10 precipitation accumulation (cm) of u200lo years (1981, 1984, 1985, 1992). (a) Observed u200lo precipitation [*Higgins et al.*, 1996]. (b) MRF u200lo precipitation. (c) Uniform resolution UGM, u200lo precipitation. The contour interval is 1 cm, and shading is for accumulation greater than or equal to 3 cm.

Fig. 11. Composite of average day 10 precipitation accumulation (cm) of all u200hi years (1950, 1952, 1969, 1996 and 2000). (a) Observed u200hi precipitation [*Higgins et al.*, 1996]. (b) Uniform resolution UGM, u200hi precipitation. (c) Two-way nested UGM, u200hi precipitation. (d) Stretched UGM, u200hi precipitation. The contour interval is 2 cm (contouring in (a) is up to 20 cm), and shading is for accumulation greater than or equal to 3 cm. The maximum observed accumulation in (a) is 24 cm.

Fig. 12. Composite of average day 10 precipitation accumulation (cm) of all u200lo years (1949, 1976, 1981, 1984, 1985 and 1992). (a) Observed u200lo precipitation [*Higgins et al.*, 1996]. (b) Uniform resolution UGM, u200lo precipitation. (c) Two-way nested UGM, u200lo precipitation. (d) Stretched UGM, u200lo precipitation. The contour interval is 1 cm, and shading is for accumulation greater than or equal to 3 cm.

Fig. 13. Time evolution of 500-mb, geopotential height anomaly correlations of the uniform resolution UGM. Correlations are computed over the Northern Hemisphere from 20°N-90°N, and over western North America from 30°N-60°N, 130°W-100°W. (a) The u200hi and u200lo composite anomaly correlations (11 cases). (b) The u200hi composite anomaly correlations (5 cases). Anomaly correlations for persistence forecasts are included.

Fig. 14. Time evolution of the composite 500-mb, geopotential height anomaly correlations from the MRF Reforecast project for winter (DJF), u200hi cases. Correlations are computed over (a) the Northern Hemisphere from 20°N-90°N, and (b) over western North America from 30°N-60°N, 130°W-100°W. The u200hi composite (line) is for forecasts initialized on 10 December 1981, 1983 and 1996; 10 January 1996 and 2000; and 10 February 1979, 1986, 1994, 1998 and 1999 (10 cases). The anomaly correlation for climatology (circles) is the average for all MRF forecasts on 10 December, January and February, from 1979-2003 (75 forecasts). Anomaly correlations for persistence forecasts are included.

Fig. 15. Time evolution of 500-mb, geopotential height anomaly correlations of the rotated, variable resolution and uniform resolution UGMs. Anomaly correlations are computed over the Northern Hemisphere from 20°N-90°N, and over western North America from 30°N-60°N, 130°W-100°W. (a) The two-way nested UGM. (b) The stretched UGM. Anomaly correlations for the uniform resolution UGM (also plotted in Fig. 13a) are included in each panel for comparison.

Fig. 16. Composite geopotential height fields (m) at 500 mb for cases of strong and weak zonal flow across the Rocky Mountains (from the NCEP/NCAR Reanalysis monthly archives). (a) Composite of u200hi cases (1950, 1952, 1969, 1996 and 2000); (b) anomalies for u200hi cases; (c) composite of u200lo cases (1949, 1976, 1981, 1984, 1985 and 1992); and (d) anomalies for u200lo cases. Anomalies in (b) and (d) are defined by subtracting the 50-year (1951-2000) January climatology of 500-mb geopotential heights from the composites in (a) and (c), respectively.

Fig. A1. Utah Global Model grid. (a) Contours of topography with uniform model resolution, 129 points in longitude, 82 points in latitude. (b) two-way nested grid. The mathematical pole has been rotated to 40°N, 110°W. Latitudinal resolution is equally spaced, 1° north of 44°N to the rotated pole, and equally spaced, 2°, south of 44°N for a total of 115 points in latitude. (c) Stretched model grid. The mathematical pole is rotated to 40°N, 110°W. Latitudinal resolution is 0.52° at the rotated north pole, and spacing increases gradually by 1% with each grid point from north to south. Latitudinal spacing is 2.3° at the rotated south pole. The total number of latitudinal points is 152. The number of points in longitude remains unchanged in (b) and (c) (129 points or 2.8° spacing). Orography contours are every 500 m, and topography higher than 2000 m is shaded.

Table 1. Ratio of area averaged u200hi to u200lo precipitation over region I denoted in Fig. 8.

Model Configuration	Day 5	Day 10	Day 15
Uniform UGM	3.0 (4.1)	2.8 (5.4)	2.4 (4.2)
MRF Reforecast	2.6 (4.9)	2.0 (7.9)	1.6 (4.2)
UGM two-way grid	3.2 (4.1)	2.3 (5.4)	1.3 (4.2)
UGM Stretched grid	3.2 (4.1)	1.9 (5.4)	1.3 (4.2)

*Parentheses denote ratio of observations.

Table 2. Ratio of area averaged u200hi to u200lo precipitation over region II denoted in Fig. 8.

Model Configuration	Day 5	Day 10	Day 15
Uniform UGM	2.1 (3.2)	2.3 (3.8)	2.1 (3.1)
MRF Reforecast	2.1 (5.4)	1.9 (7.0)	1.5 (3.3)
UGM two-way grid	1.8 (3.2)	1.6 (3.8)	1.2 (3.1)
UGM Stretched grid	1.9 (3.2)	1.3 (3.8)	1.4 (3.1)

*Parentheses denote ratio of observations.

Table 3. Ratio of area averaged u200hi to u200lo precipitation over regions III and IV denoted in Fig. 8.

Model Configuration	Day 5	Day 10	Day 15
Uniform UGM	3.8 (4.3)	3.1(6.4)	2.4 (4.8)
MRF Reforecast	3.7 (2.6)	2.2 (7.1)	1.6 (5.0)
UGM two-way grid	7.2 (4.3)	3.3 (6.4)	1.4 (4.8)
UGM Stretched grid	7.1 (4.3)	3.1 (6.4)	1.2 (4.8)

*Parentheses denote ratio of observations.

Table 4. Ratio of area averaged u200hi to u200lo precipitation over region III denoted in Fig. 8.

Model Configuration	Day 5	Day 10	Day 15
Uniform UGM	6.9 (20.2)	4.4 (14.4)	3.2 (7.9)
MRF Reforecast	6.9 (14.5)	2.5 (13.8)	1.8 (6.7)
UGM two-way grid	12.8 (20.2)	3.7 (14.4)	1.4 (7.9)
UGM Stretched grid	13.8 (20.2)	3.6 (14.4)	1.3 (7.9)

*Parentheses denote ratio of observations.

Table 5. Ratio of area averaged u200hi to u200lo precipitation over region IV denoted in Fig. 8.

Model Configuration	Day 5	Day 10	Day 15
Uniform UGM	1.9 (0.9)	1.9 (2.0)	1.5 (1.9)
MRF Reforecast	1.7 (0.6)	1.8 (2.3)	1.3 (2.4)
UGM two-way grid	3.8 (0.9)	2.6 (2.0)	1.6 (1.9)
UGM Stretched grid	3.4 (0.9)	2.3 (2.0)	1.0 (1.9)

*Parentheses denote ratio of observations.

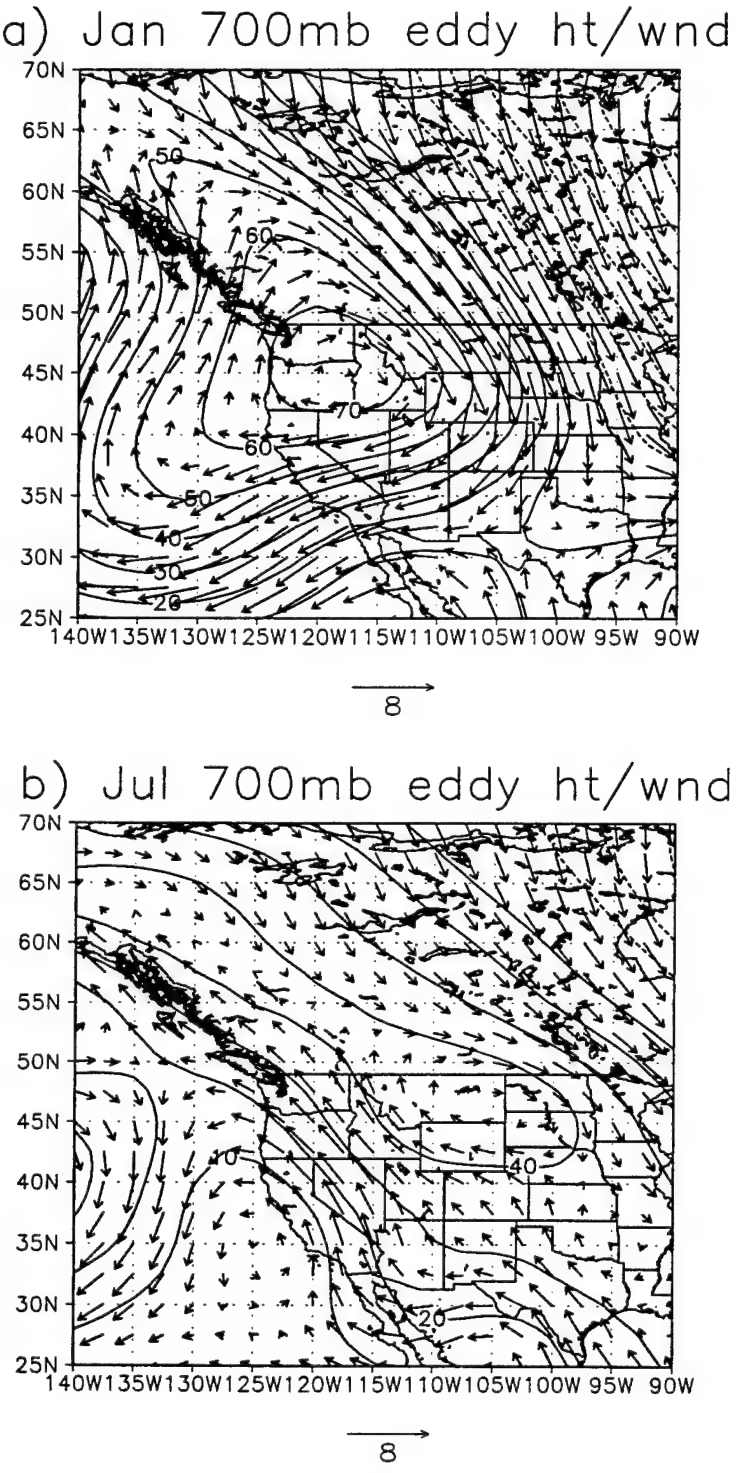

FIG. 1. Climatology of 700-mb eddy heights (m) and wind vectors (m/s) over North America for (a) January; and (b) July from the NCEP/NCAR Reanalysis monthly archive. Eddies are defined by removing the zonal average.

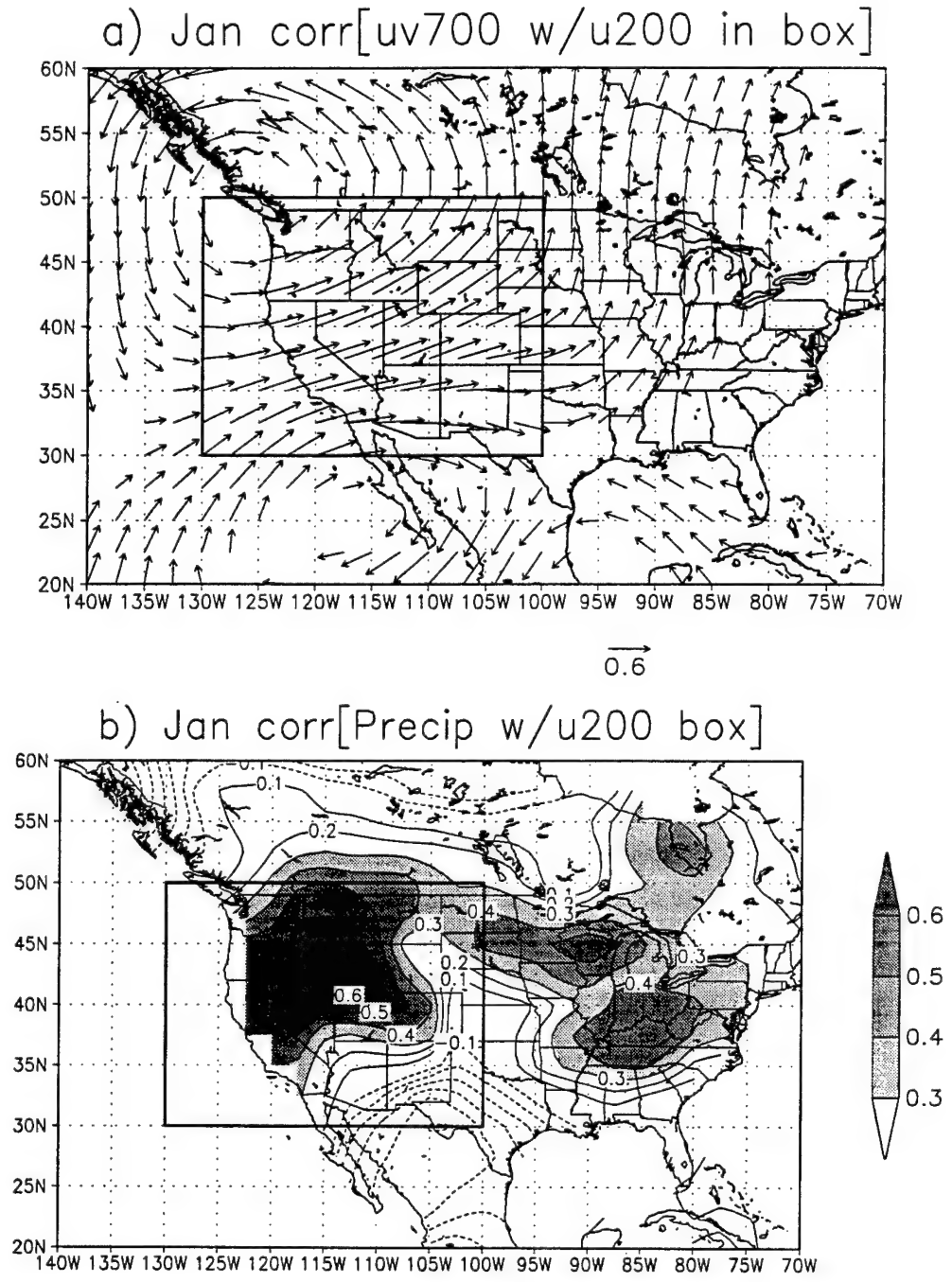

FIG. 2. Time correlation over North America (1951-2000) during January. (a) Correlation vectors of the area-averaged, 200-mb zonal wind in the outlined box (30°N-50°N, 130°W-100°W) with 700-mb wind at all locations. (b) Similar to (a), but 200-mb, zonal wind in the outlined box is correlated with precipitation over land (PREC/L of *Chen et al.*, 2002). The magnitude of correlation vectors is indicated at the bottom of panel (a), and only coefficients meeting the 99% statistical significance criteria (0.3) are plotted. Positive correlation coefficients greater than 0.3 are shaded in (b).

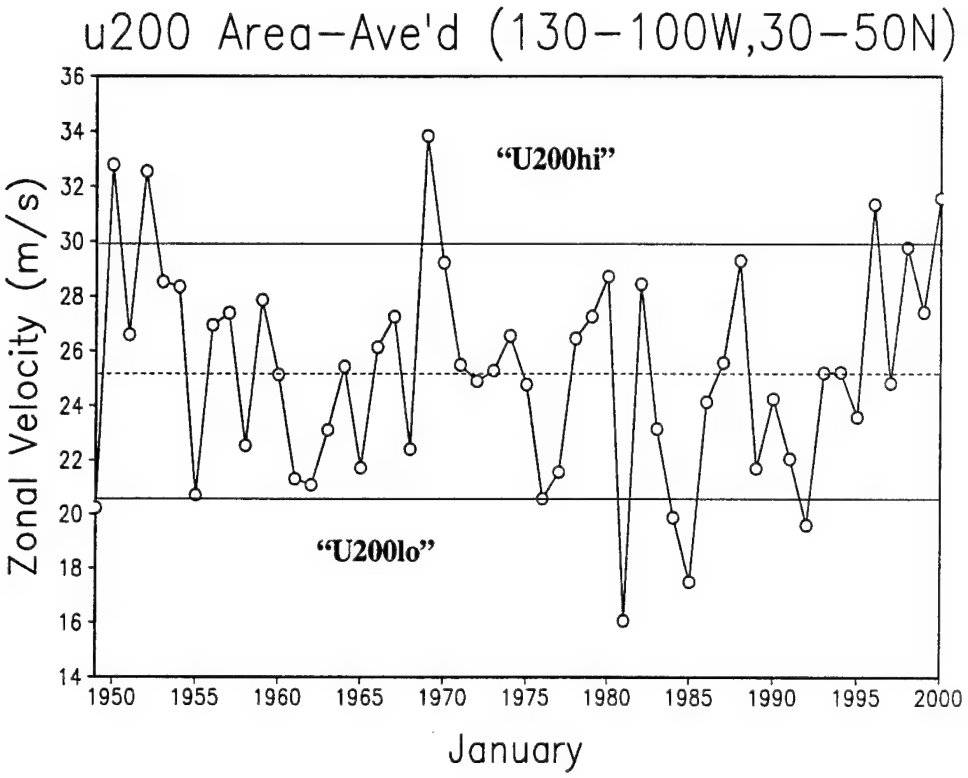

FIG. 3. Climatology of the area averaged, 200-mb zonal flow over western North America during January (30°N-50°N, 130°W-100°W), 1949-2000. The dashed horizontal line indicates the 52 year mean (25.2 m/s). Solid lines are drawn to indicate plus and minus 1.2 times the standard deviation from the mean.

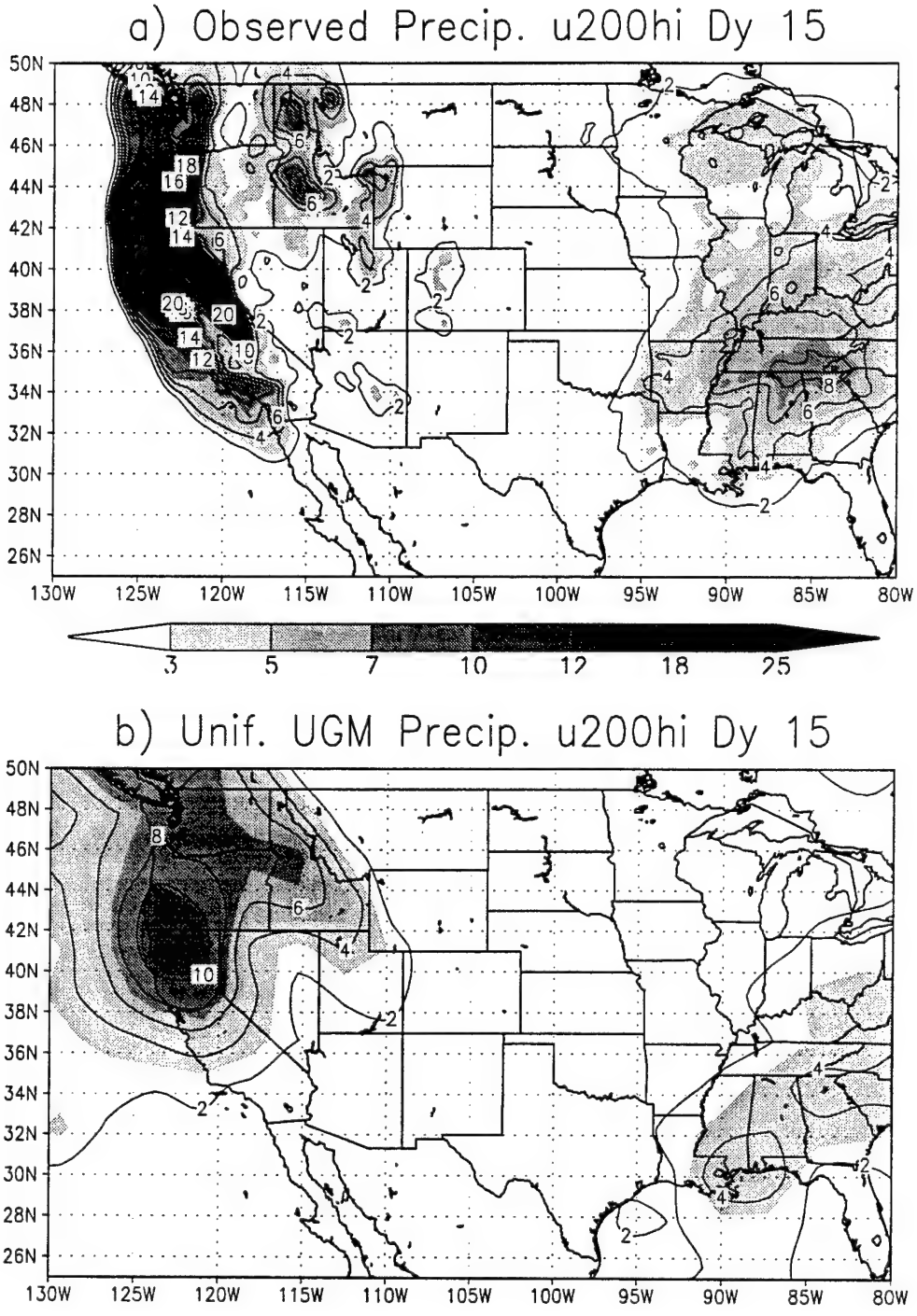

FIG. 4. Average precipitation accumulation for the five u200hi composites (cm). (a) Observed, 15 day accumulation (10-24 January 1950, 1952, 1969, 1996 and 2000). (b) 15 day accumulation of the uniform resolution UGM. The contour interval is 2 cm in (a) and (b) (contouring in (a) is up to 20 cm). Shading is for accumulation greater than or equal to 3 cm. The maximum observed accumulation in (a) is 33 cm.

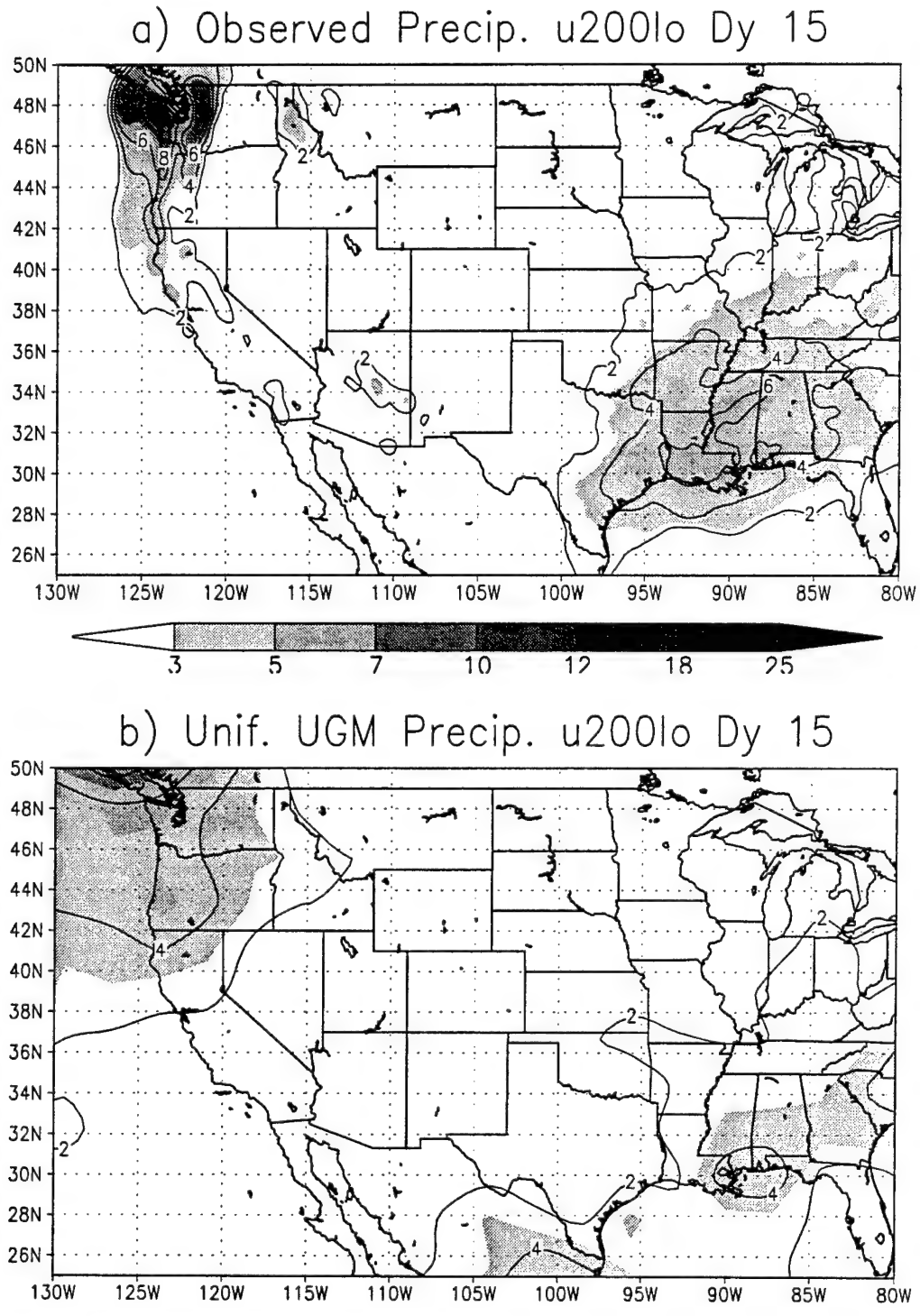

FIG. 5. Average precipitation accumulation for the six u200lo composites (cm). (a) Observed, 15 day accumulation (10-24 January 1949, 1976, 1981, 1984, 1985 and 1992). (b) 15 day accumulation of the uniform resolution UGM. The contour interval is 1 cm in (a) and (b). Shading is for accumulation greater than or equal to 3 cm.

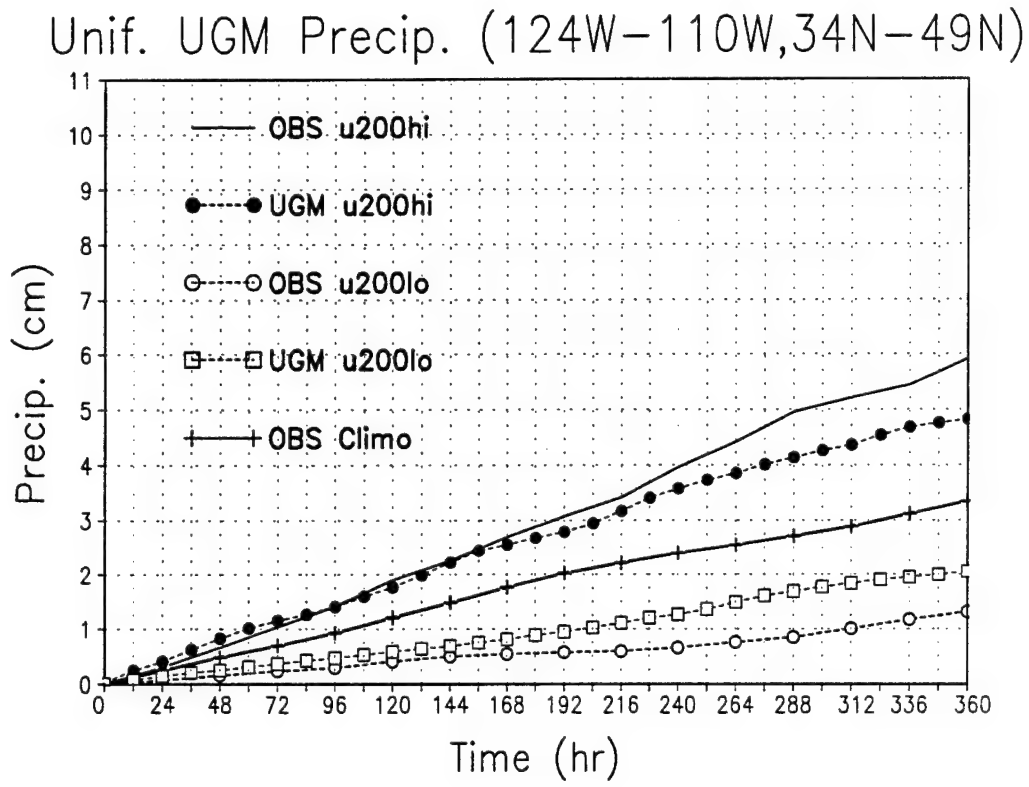

FIG. 6. Composite u200hi and u200lo, area averaged precipitation accumulation (cm) (124°W-110°W, 34°N-49°N) from observations and the uniform resolution UGM. Time 0 is on 10 January. Observations are from the CPC Unified data set [*Higgins et al.*, 1996]. The line labelled with (+) marks indicates the 30 year CPC climatology of 10-24 January precipitation accumulation over the same region from 1970-2000 (excluding 1973).

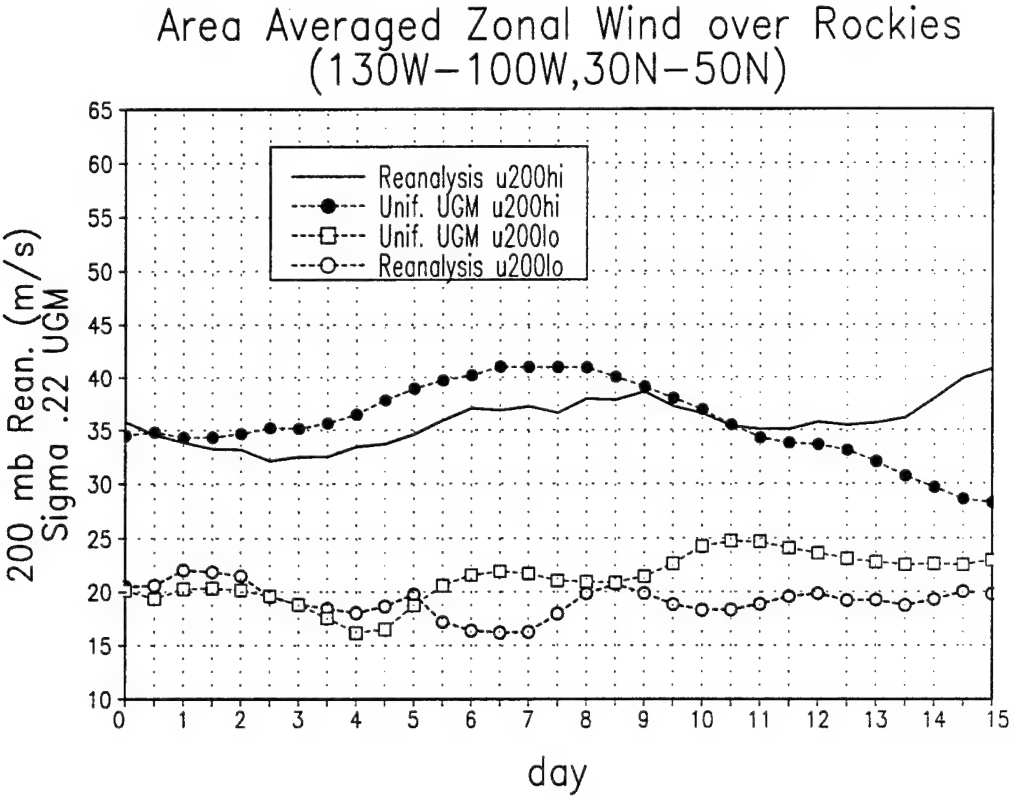

FIG. 7. Composite u200hi and u200lo, area averaged, upper troposphere zonal wind (m/s) (130°W-100°W, 30°N-50°N) from the NCEP/NCAR Reanalysis and the uniform resolution UGM. The 200-mb zonal flow is plotted for the NCEP/NCAR Reanalysis, and the sigma level 0.22 zonal flow is plotted for the uniform resolution UGM.

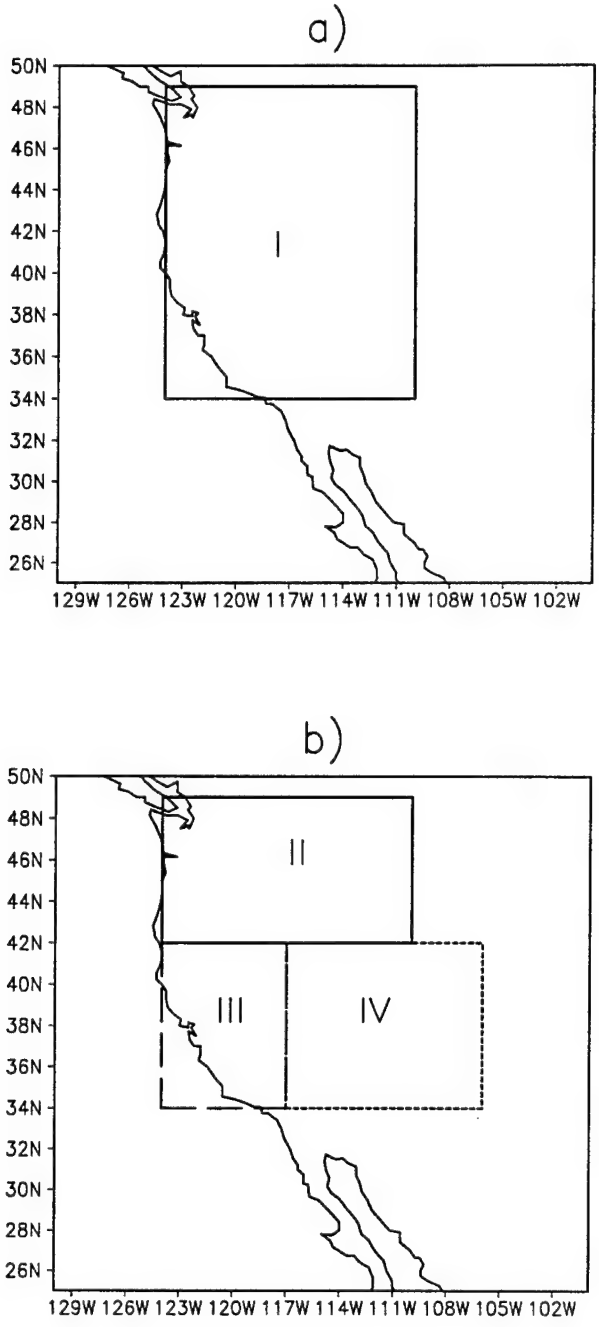

FIG. 8. Regions over which the area average precipitation accumulation is calculated for model forecast comparisons. (a) Region I (western U.S.); (b) region II (northern states); (c) region III (California, Nevada); and (d) region IV (Colorado River basin).

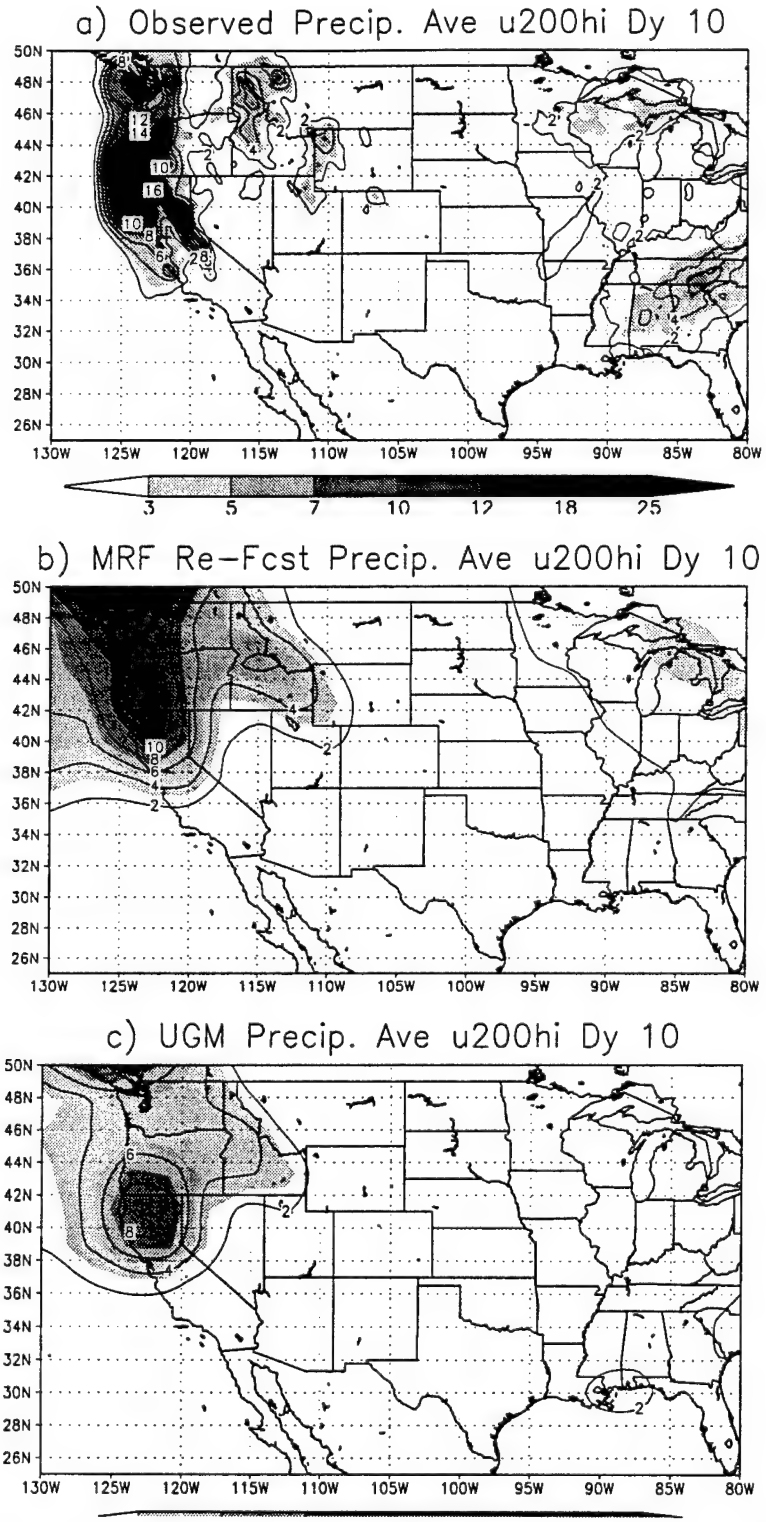

FIG. 9. Composite of average day 10 precipitation accumulation (cm) of u200hi years (1996 and 2000). (a) Observed u200hi precipitation (Higgins et al., 1996). (b) MRF u200hi precipitation. (c) Uniform resolution UGM, u200hi precipitation. The contour interval is 2 cm (contouring in (a) is up to 20 cm), and shading is for accumulation greater than or equal to 3 cm. The maximum observed accumulation in (a) is 24 cm.

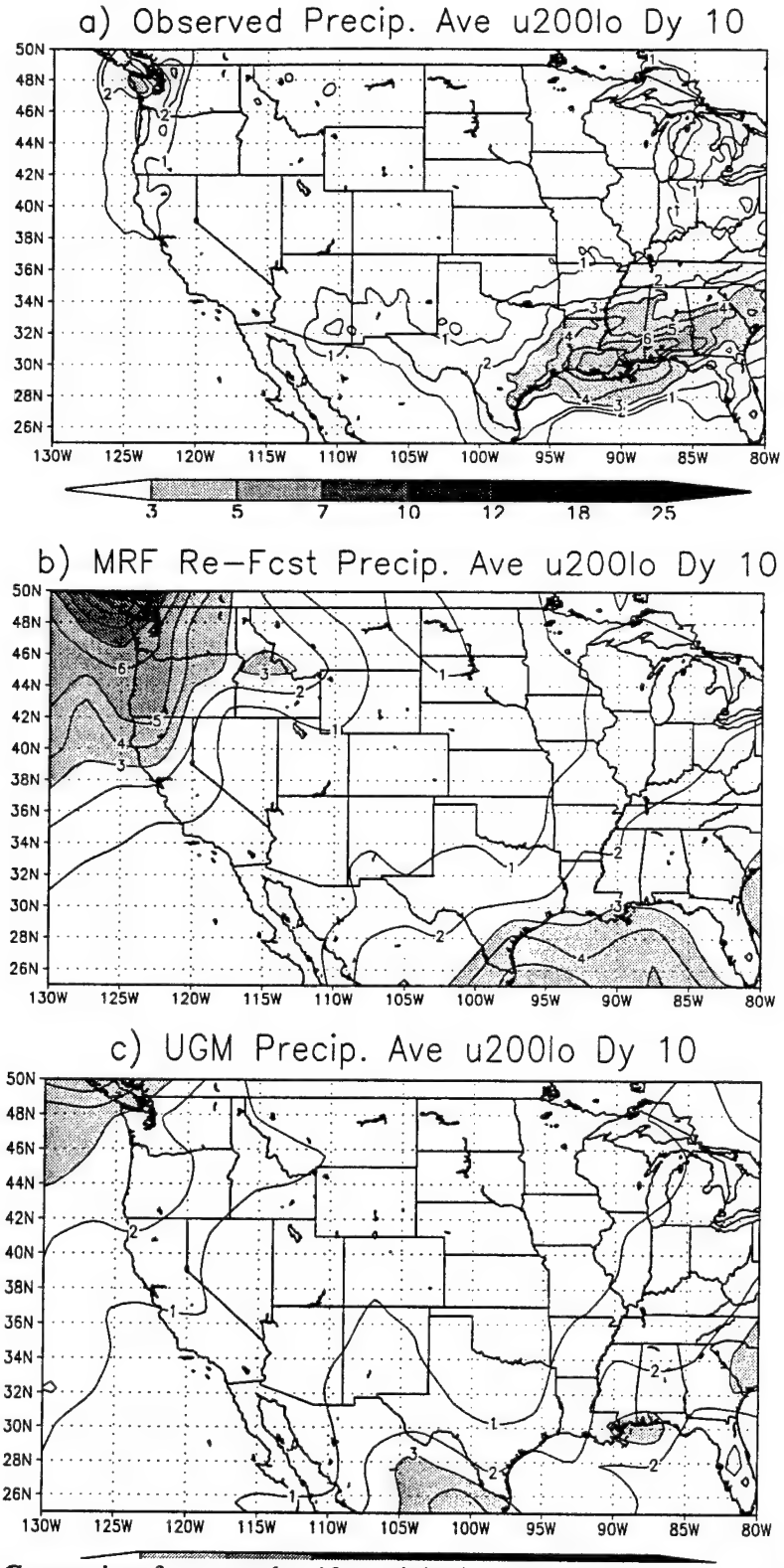

FIG. 10. Composite of average day 10 precipitation accumulation (cm) of u200lo years (1981, 1984, 1985, 1992). (a) Observed u200lo precipitation [*Higgins et al.*, 1996]. (b) MRF u200lo precipitation. (c) Uniform resolution UGM, u200lo precipitation. The contour interval is 1 cm, and shading is for accumulation greater than or equal to 3 cm.

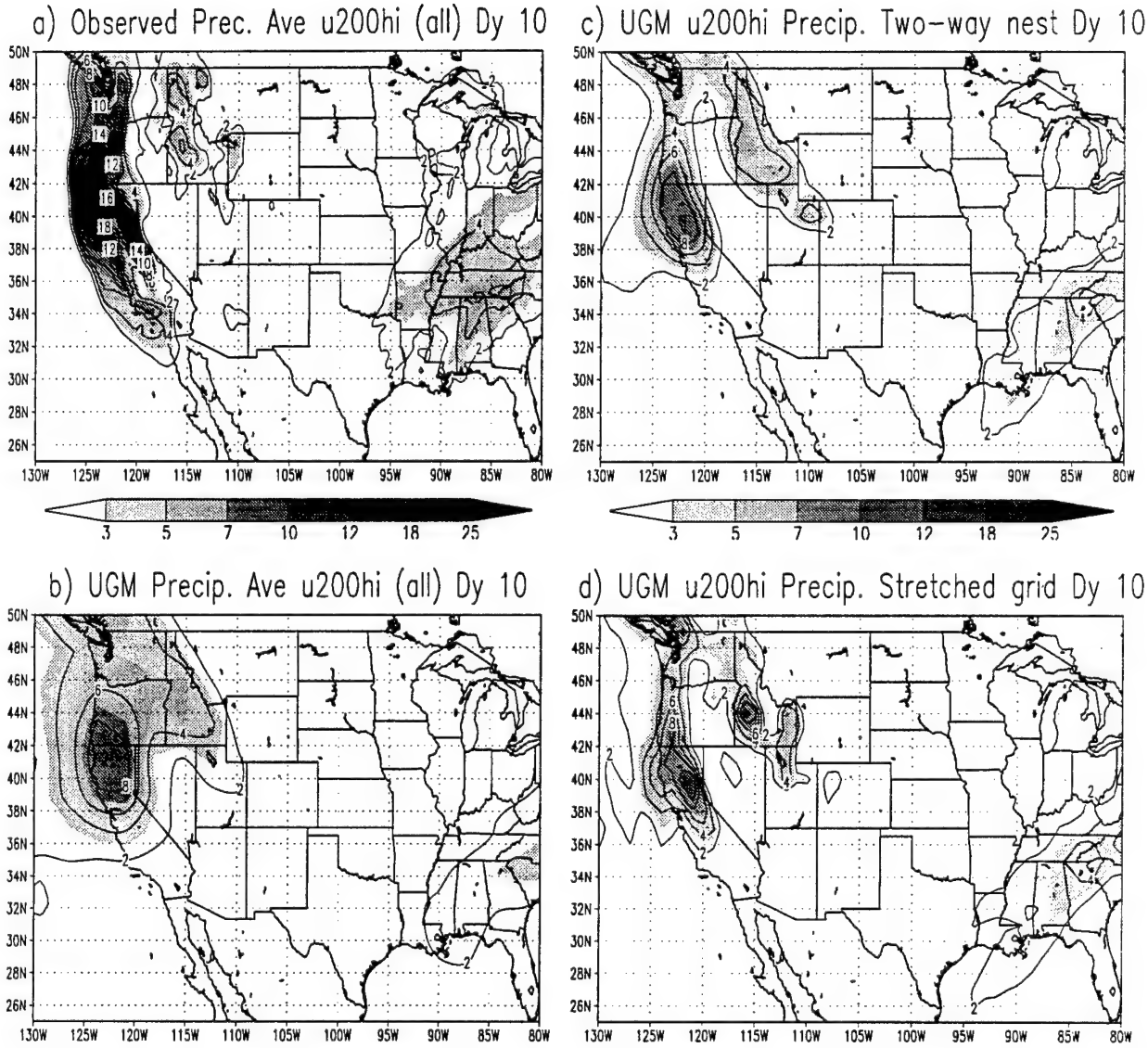

FIG. 11. Composite of average day 10 precipitation accumulation (cm) of all u200hi years (1950, 1952, 1969, 1996 and 2000). (a) Observed u200hi precipitation [*Higgins et al.*, 1996]. (b) Uniform resolution UGM, u200hi precipitation. (c) Two-way nested UGM, u200hi precipitation. (d) Stretched UGM, u200hi precipitation. The contour interval is 2 cm (contouring in (a) is up to 20 cm), and shading is for accumulation greater than or equal to 3 cm. The maximum observed accumulation in (a) is 24 cm.

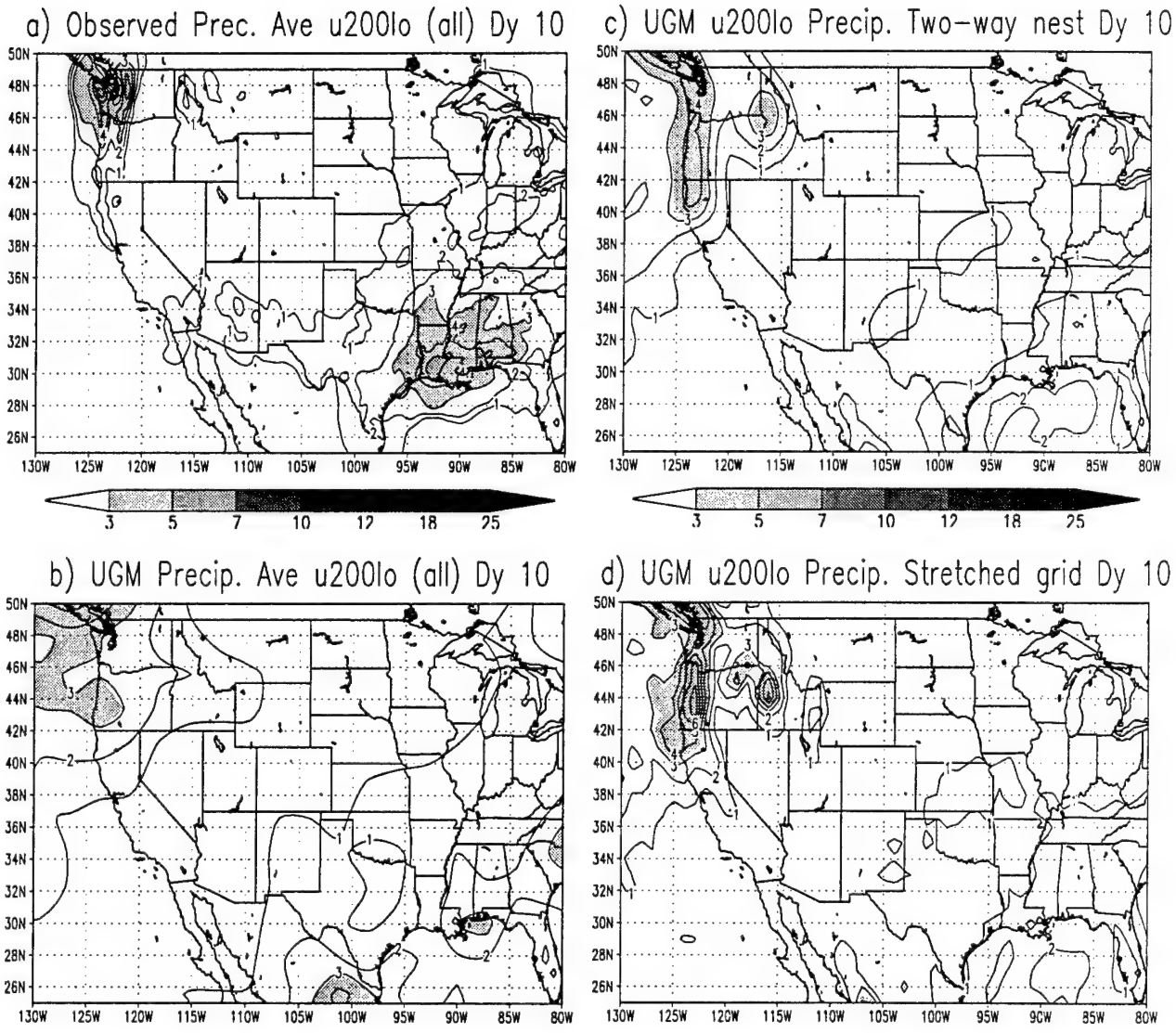

FIG. 12. Composite of average day 10 precipitation accumulation (cm) of all u200lo years (1949, 1976, 1981, 1984, 1985 and 1992). (a) Observed u200lo precipitation [*Higgins et al.*, 1996]. (b) Uniform resolution UGM, u200lo precipitation. (c) Two-way nested UGM, u200lo precipitation. (d) Stretched UGM, u200lo precipitation. The contour interval is 1 cm, and shading is for accumulation greater than or equal to 3 cm.

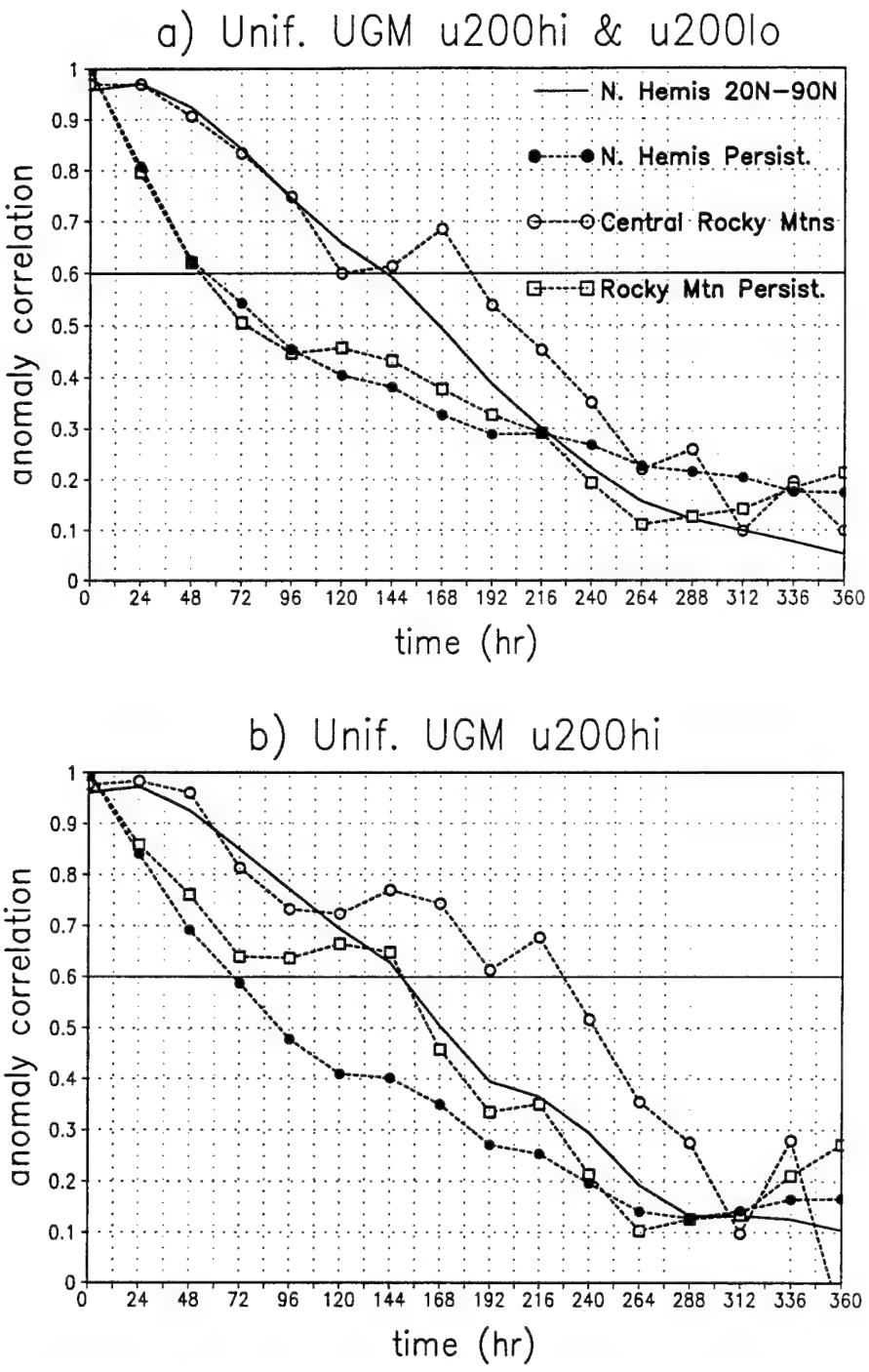

FIG. 13. Time evolution of 500-mb, geopotential height anomaly correlations of the uniform resolution UGM. Correlations are computed over the Northern Hemisphere from 20°N-90°N, and over western North America from 30°N-60°N, 130°W-100°W. (a) The u200hi and u200lo composite anomaly correlations (11 cases). (b) The u200hi composite anomaly correlations (5 cases). Anomaly correlations for persistence forecasts are included.

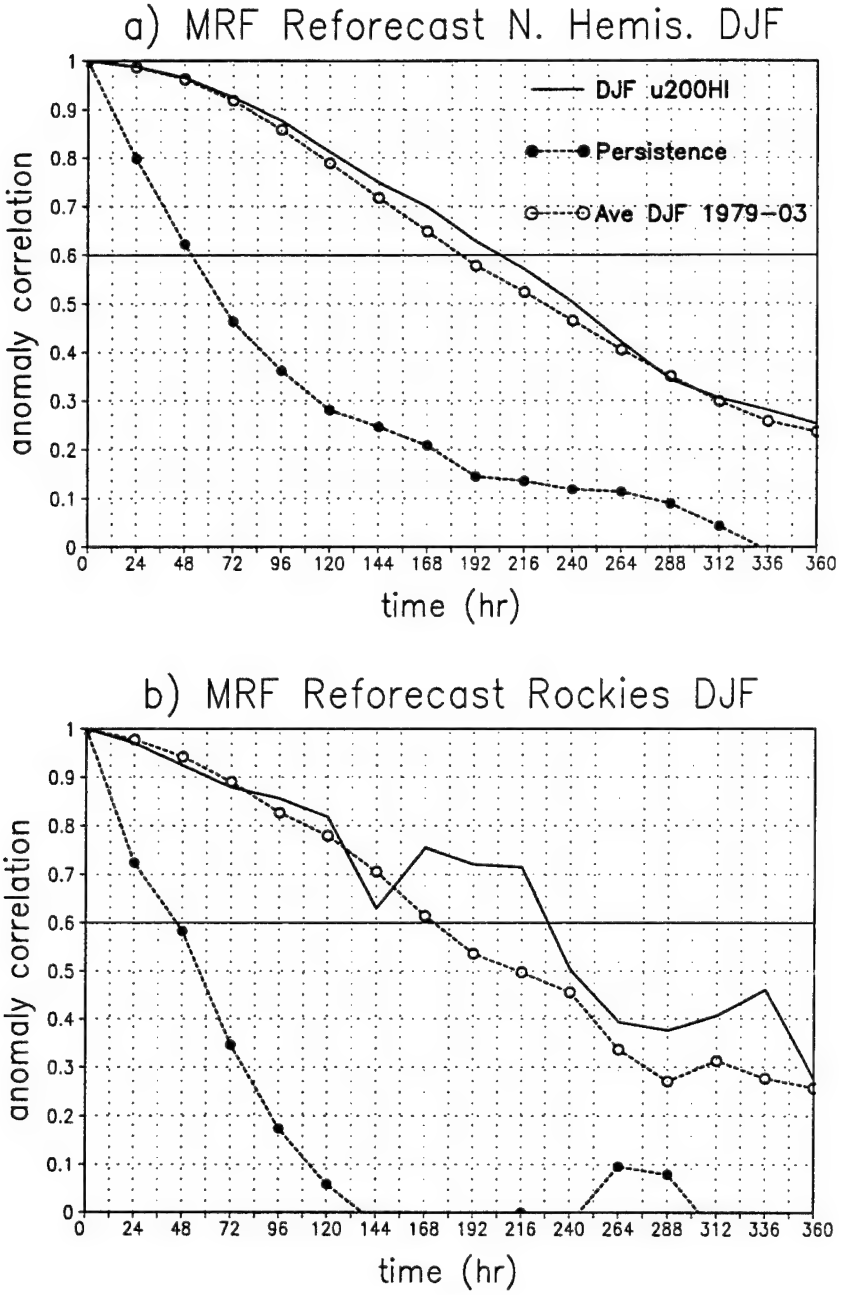

FIG. 14. Time evolution of the composite 500-mb, geopotential height anomaly correlations from the MRF Reforecast project for winter (DJF), u200hi cases. Correlations are computed over (a) the Northern Hemisphere from 20°N-90°N, and (b) over western North America from 30°N-60°N, 130°W-100°W. The u200hi composite (line) is for forecasts initialized on 10 December 1981, 1983 and 1996; 10 January 1996 and 2000; and 10 February 1979, 1986, 1994, 1998 and 1999 (10 cases). The anomaly correlation for climatology (circles) is the average for all MRF forecasts on 10 December, January and February, from 1979-2003 (75 forecasts). Anomaly correlations for persistence forecasts are included.

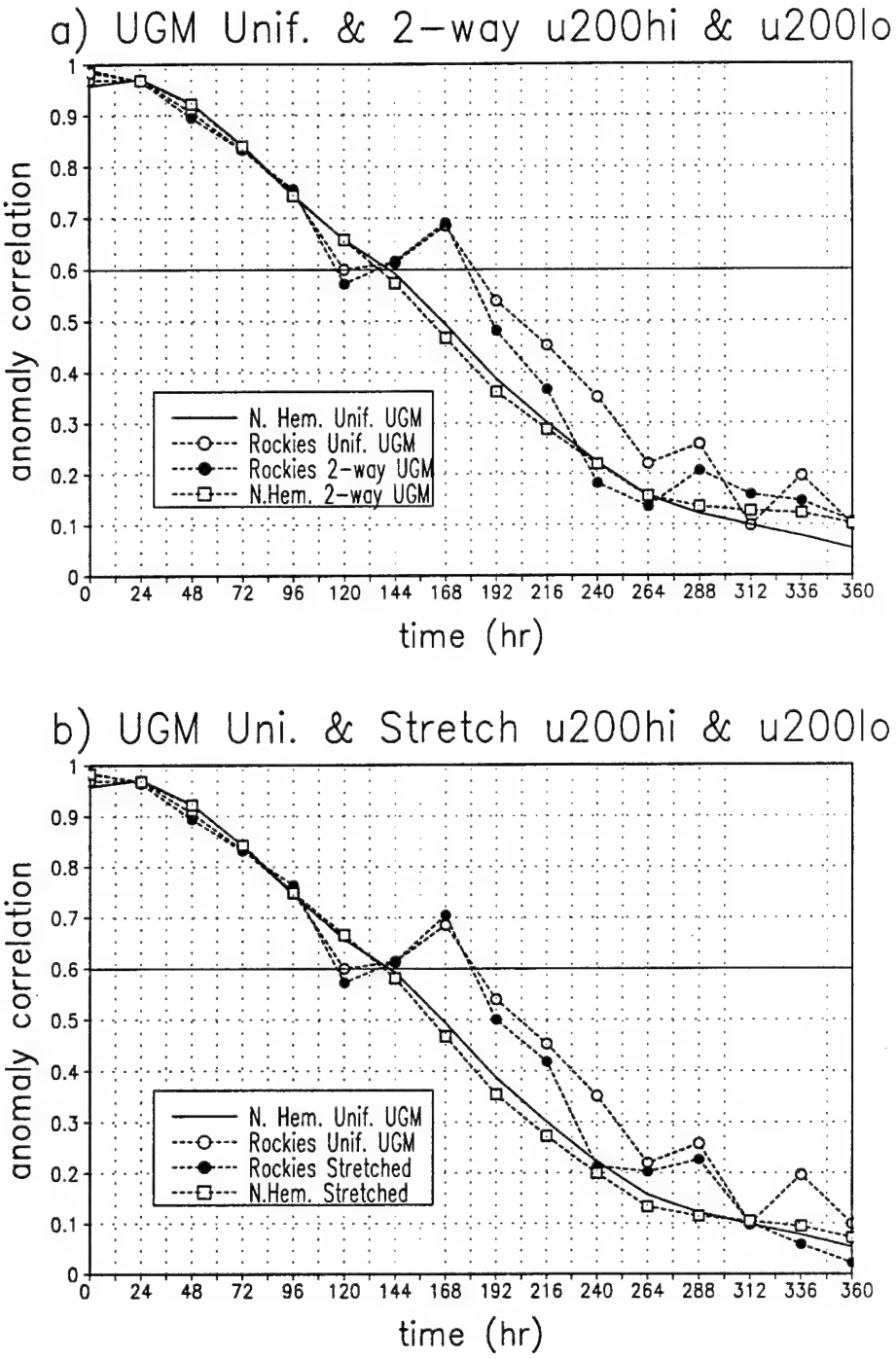

FIG. 15. Time evolution of 500-mb, geopotential height anomaly correlations of the rotated, variable resolution and uniform resolution UGMs. Anomaly correlations are computed over the Northern Hemisphere from 20°N-90°N, and over western North America from 30°N-60°N, 130°W-100°W. (a) The two-way nested UGM. (b) The stretched UGM. Anomaly correlations for the uniform resolution UGM (also plotted in Fig. 13a) are included in each panel for comparison.

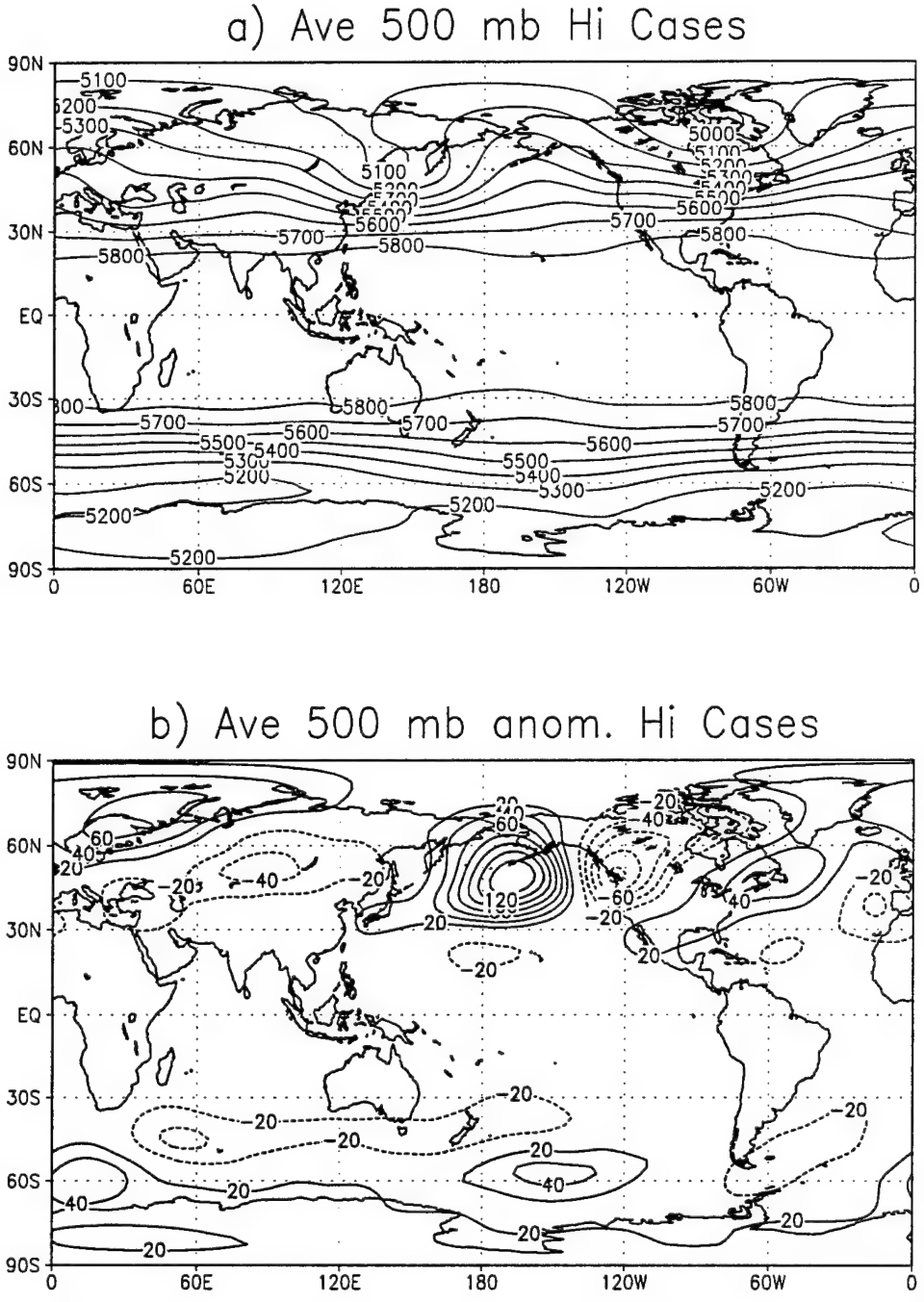

FIG. 16. Composite geopotential height fields (m) at 500 mb for cases of strong and weak zonal flow across the Rocky Mountains (from the NCEP/NCAR Reanalysis monthly archives). (a) Composite of u200hi cases (1950, 1952, 1969, 1996 and 2000); (b) anomalies for u200hi cases; (c) composite of u200lo cases (1949, 1976, 1981, 1984, 1985 and 1992); and (d) anomalies for u200lo cases. Anomalies in (b) and (d) are defined by subtracting the 50-year (1951-2000) January climatology of 500-mb geopotential heights from the composites in (a) and (c), respectively.

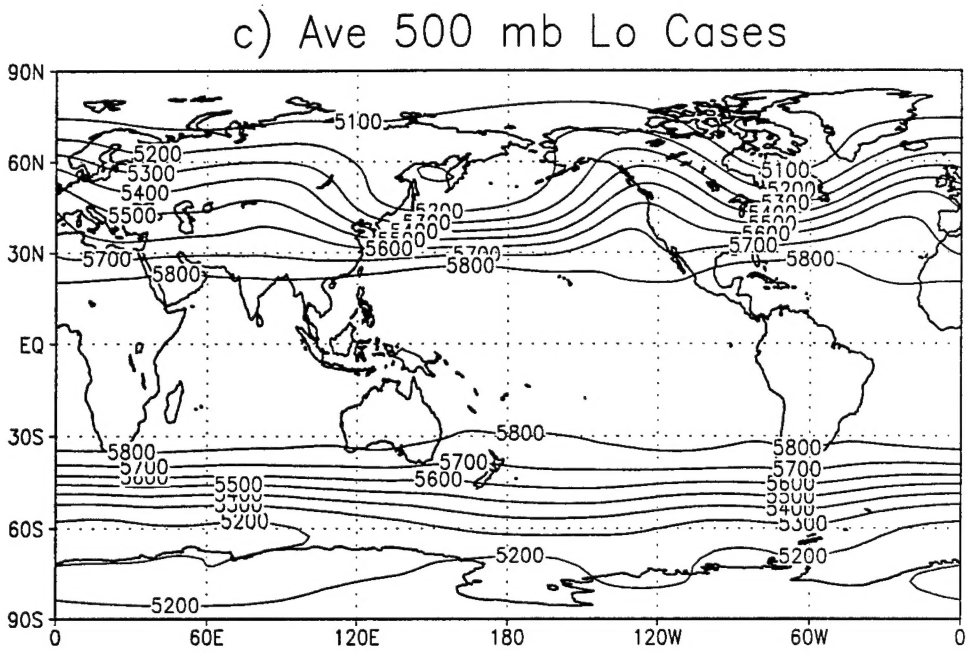

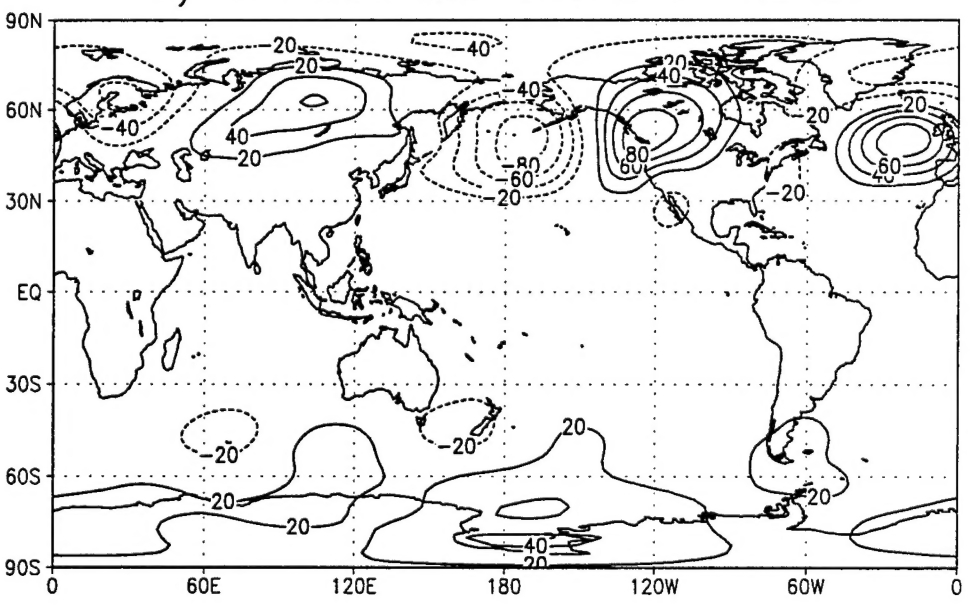

Fig. 16, continued.

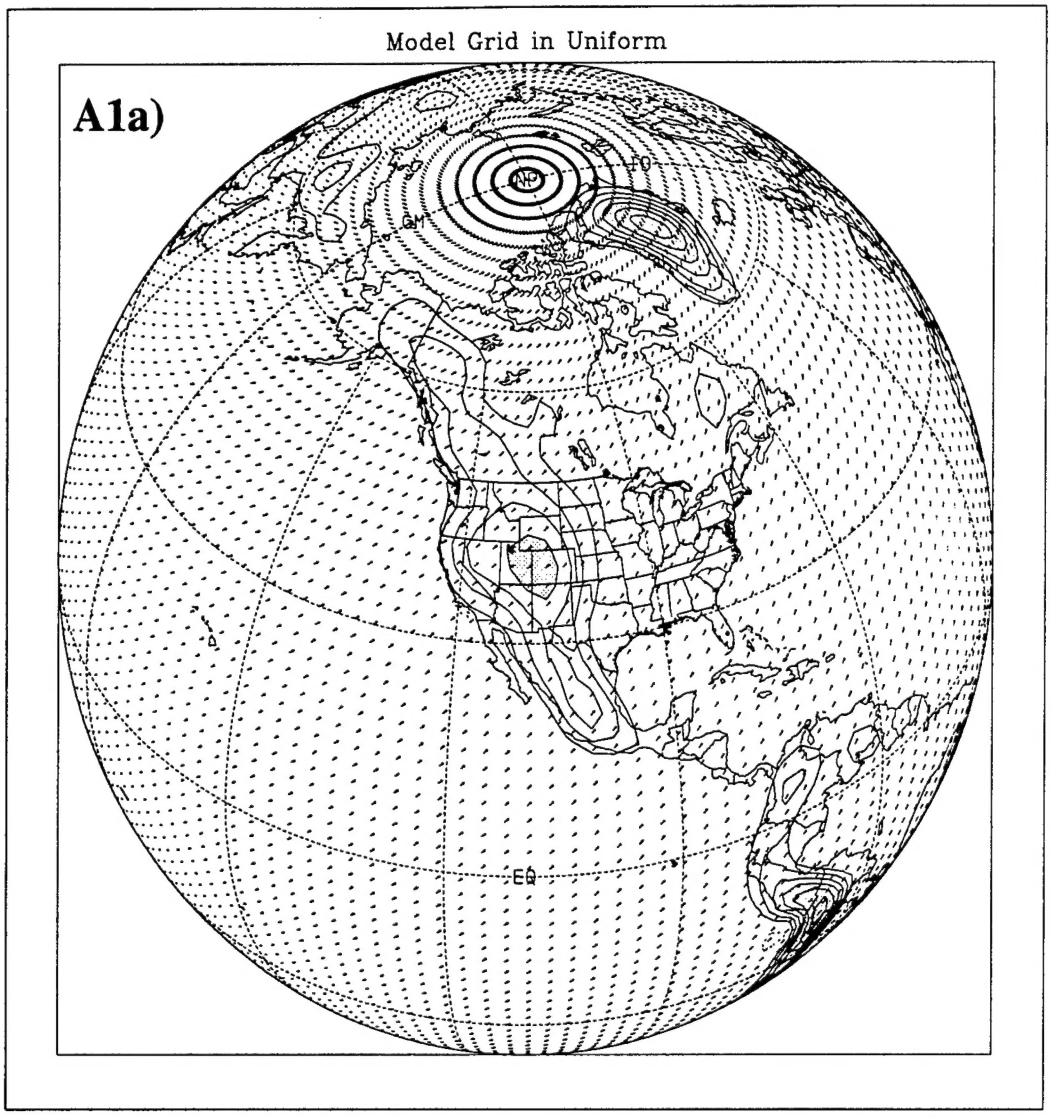

Fig. A1. Utah Global Model grid. (a) Contours of topography with uniform model resolution, 129 points in longitude, 82 points in latitude. (b) two-way nested grid. The mathematical pole has been rotated to 40°N, 110°W. Latitudinal resolution is equally spaced, 1° north of 44°N to the rotated pole, and equally spaced, 2°, south of 44°N for a total of 115 points in latitude. (c) Stretched model grid. The mathematical pole is rotated to 40°N, 110°W. Latitudinal resolution is 0.52° at the rotated north pole, and spacing increases gradually by 1% with each grid point from north to south. Latitudinal spacing is 2.3° at the rotated south pole. The total number of latitudinal points is 152. The number of points in longitude remains unchanged in (b) and (c) (129 points or 2.8° spacing). Orography contours are every 500 m, and topography higher than 2000 m is shaded.

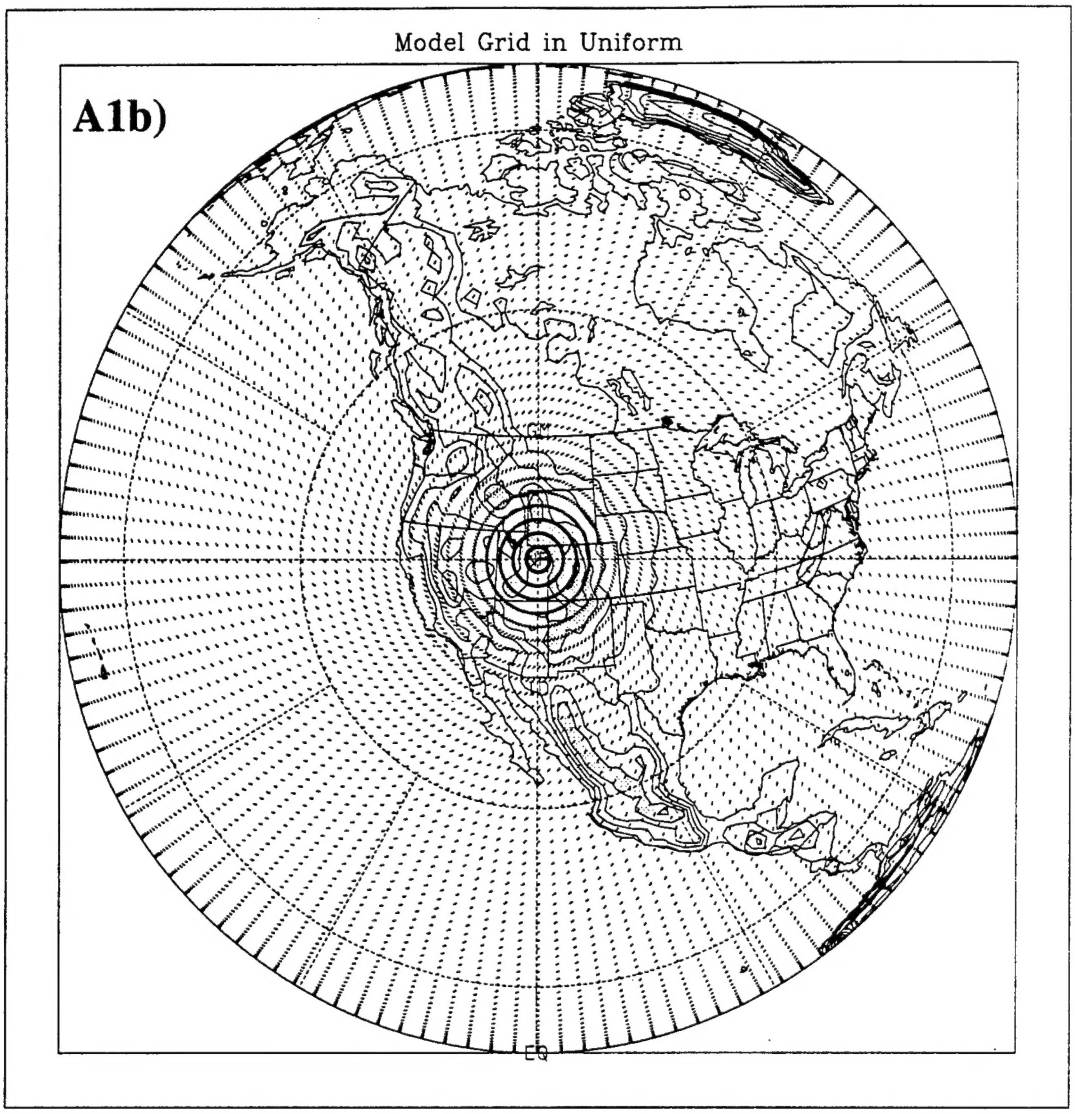

Fig. A1, continued.

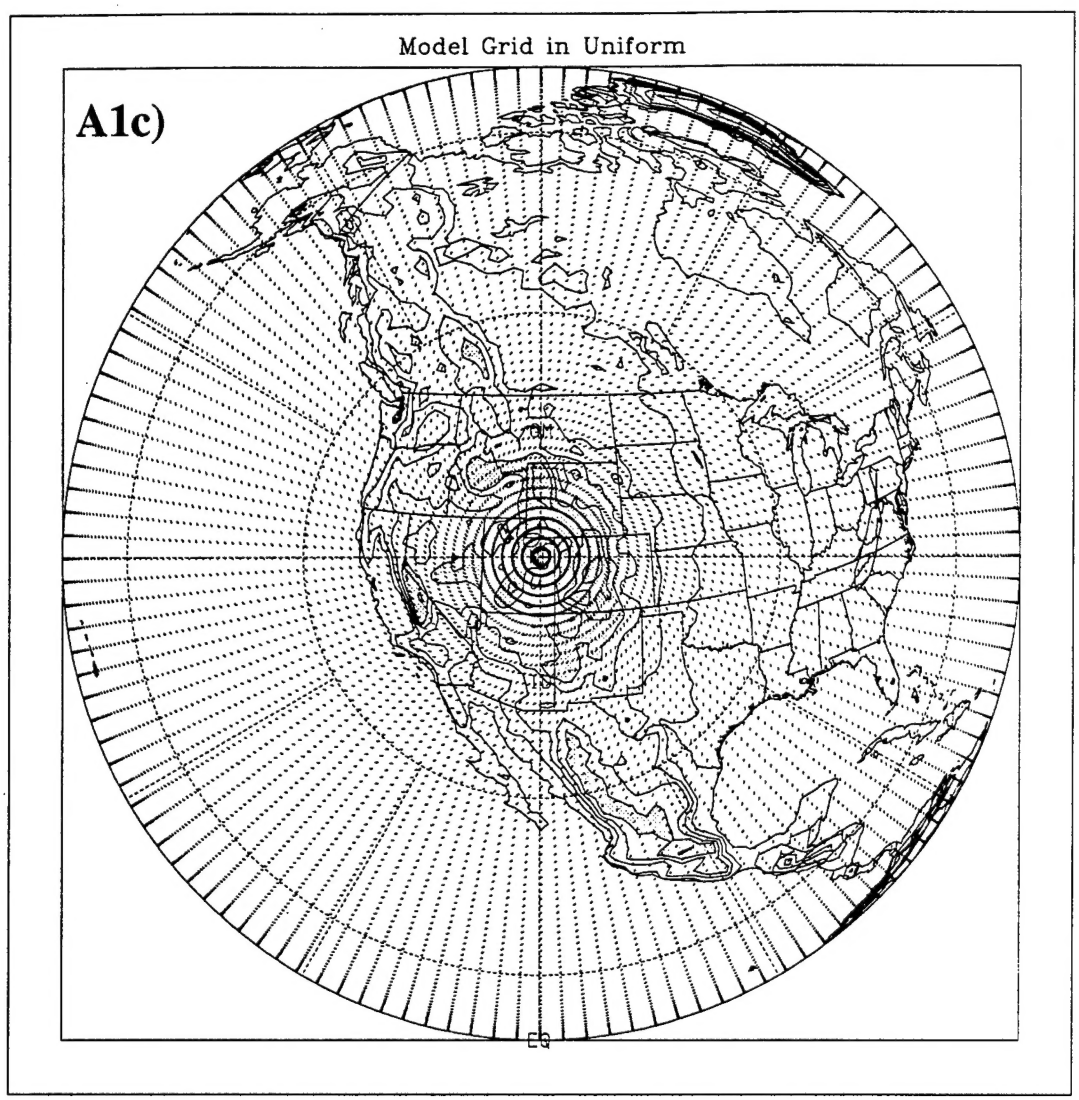

Fig. A1, continued.